THE ELASTIC MECHANICAL PROPERTIES OF SUPPORTED THIN POLYMER FILMS

By

Peter C. Chung

A dissertation submitted in partial fulfillment
of the requirements for the degree of
Doctor of Philosophy
(Materials Science and Engineering)
in the University of Michigan
2015

Doctoral Committee:

Professor Peter F. Green, Chair
Professor Michael Atzmon
Professor Richard E. Robertson
Professor Michael J. Solomon

To my wife, my parents, and my brothers

Acknowledgements

I would like to acknowledge the following people who influenced and helped me throughout the process of my doctoral study. First of all, I would like to express my deep gratitude to my research advisor Professor Peter F. Green for his support, guidance, and patience throughout my doctoral study. Professor Green supported me to work on research projects I was highly interested in, and encouraged my research by providing deep scientific insights to understand new findings. I would also like to thank my committee members Professor Michael Atzmon, Professor Richard Robertson, and Professor Michael J. Solomon. Their comments and suggestions during my preliminary exam and data meeting helped me to shape the research direction of my doctoral study and elaborate my work.

I need to thank my former and current colleagues within the Green group. I would miss years of memories we share together on discussing about our research, providing technical help to solve problems, congratulating new publications, and cheering each other when things were not going smooth. I especially thank Dr. Emmanouil Glynos for his help and support throughout my Ph.D. study. He extensively helped me to design an atomic force microscopy based nanoindentation technique. I also need to thank all the other group members of the Green group for their help and support as a colleague and as well as a friend: Dr. Aaron Tan, Dr. Chelsea Chen, Dr. Jenny Kim, Dr. Bradley Frieberg,

Dr. Hengxi Yang, Dr. Bingyuan Huang, Jojo Amonoo, Ravi Sharma, Kyle Johnson, Anton Li, Jill Wenderott, Junnan Zhao, and Ban Dong.

For the last, I would like to express my greatest thanks to my family. I cannot imagine getting through all the difficulties and problems I have experienced during my Ph.D. study without warm and endless support from my family. I would like to thank my loving wife, Mihyun Kim, for her unconditional love and support. I would also like to thank my parents, Kyung-soo Chung, Eun-hee Lee, my brothers, John Chung, and Myungwoo Chung, for their support and encouragement throughout this process. I would also like to thank my in-laws for unwavering support and understanding.

Table of Contents

Dedication ..... **ii**

Acknowledgements ..... **iii**

List of Figures ..... **viii**

List of Appendices ..... **xii**

Abstract ..... **xiii**

Chapter 1 Introduction **1**

1.1 Motivation and Research Objectives 1

1.2 Background 4

1.2.1 Principle of AFM Nanoindentation *4*

1.2.2 Elastic Contact Mechanics Models *7*

1.3 Viability of the AFM Nanoindentation Technique 9

1.4 References 11

Chapter 2 The Elastic Mechanical Response of Supported Thin Polymer Films **15**

2.1 Introduction 15

2.2 Experimental Section 18

2.2.1 Sample Preparation *18*

2.2.2 Atomic Force Microscope *19*

2.2.3 Elastic Contact Mechanical Model *19*

2.2.4 Finite Element Analysis *20*

2.3 Results and Discussion 21

2.4 Conclusion 31

2.5 References 32

Chapter 3 The Elastic Mechanical Response of Nanoscale Thin Films of Miscible Polymer/Polymer Blends 37

3.1 Introduction 37

3.2 Experimental Section 41

3.3 Results and Discussion 43

3.4 Conclusion 55

3.5 References 56

Chapter 4 Macromolecular Architecture Influences the Elastic Mechanical Response of Thin Supported Polymer Films 61

4.1 Introduction 61

4.2 Experimental Section 64

4.3 Results and Discussion 67

4.4 Conclusion 73

4.5 References 73

Chapter 5 Conclusions..... 77

Appendices……..……...80

List of Figures

Figure 1.1 A schematic image of typical AFM components is shown..... 6

Figure 1.2 A schematic image showing different steps of a FD curve. 7

Figure 1.3 (a) Same set of FD curves was fitted with the Hertz model (filled squares) and JKR model (filled triangles) and the effective moduli, E, are plotted as a function of maximum force, F_{max}. Each data point is an average of 3 nanoindentation measurements. (b) The corresponding indentation depths, d, from data shown in part (a) are plotted with open symbols as a function of F_{max}. Each data point is an average of 3 nanoindentation measurements. (c) The relative underestimation of d (ratio of d estimated by the JKR and Hertz models) is shown as a function of F_{max}. 10

Figure 2.1 Typical FD curve obtained from an AFM nanoindentation measurement on $h \sim 1$ μm PS film fitted with the JKR model: approach curve (open squares), retraction curve (open circles), and the JKR fitting (solid line). Note that the approach and retraction curves overlap without hysteresis, indicating the deformation behavior is purely elastic. 21

Figure 2.2 (a) Effective moduli, $E(h)$, for PMMA, PS, PC, and PVC films at fixed maximum force, F_{max}, of 400 nN plotted as a function of film thickness, h; dashed lines are guides for the eyes. (b) $E(h)$ normalized with average

effective moduli for $h > h_t$, $E(h > h_t)$, and plotted as a function of ratio of contact radius to film thickness, a/h. Each data point is an average of 10 nanoindentation measurements, and dashed lines are guides for the eyes. ……24

Figure 2.3 Effective moduli, E, for PMMA, PC, and PVC films with similar film thickness, h ~ 320 nm, as a function of F_{max} from 300 nN up to 700 nN. Each data point is an average of three nanoindentation measurements, and dashed lines are guides for the eyes. 27

Figure 2.4 Normalized effective moduli, $E(h)/E_{polymer}$, are plotted as a function of a/h. $E_{polymer}$ were taken from our experimental results (E_{PMMA} = 5.9 GPa, E_{PS} = 5.2 GPa, E_{PC} = 3.0 GPa, and E_{PVC} = 3.9 GPa) and Poisson's ratios were taken from the literature ($\nu_{PMMA} = \nu_{PS} = 0.33$, $\nu_{PC} = 0.37$, and $\nu_{PVC} = 0.38$). Note that the moduli curves almost overlay regardless of differences in the elastic modulus and Poisson's ratio of the simulated films. Insets show the indentation-induced stress field under the indentation center for h = 1000 nm, h = 400 nm, and h = 200 nm films (from left to right) for simulated PMMA films. Meshes are not shown for visual clarity. 28

Figure 3.1 (a) A typical FD curve obtained from a nanoindentation measurement of a film of h ~ 620 nm thick TMPC film is shown. (b) The K is shown for PS and TMPC films. Each data point is an average of 11 nanoindentation experiments, and the dashed lines are guides for the eyes. 45

Figure 3.2 K of the PS/TMPC blend films of thickness, h ~ 620 nm, at fixed maximum force, F_{max} = 400 nN, are plotted as a function of the weight fraction of TMPC, ϕ. Each data point is an average of 15 nanoindentation measurements, and the dashed line is guide for the eyes. 47

Figure 3.3 (a) Effective reduced moduli, $K(h)$, for PS, a 50/50 wt % blend of PS/TMPC, and TMPC films are plotted as a function of film thickness, h. (b) $K(h)$ normalized with average effective moduli for $h > h_t$, $K(h > h_t)$, and plotted as a function of ratio of contact radius to film thickness, a/h. The maximum force, F_{max}, was kept at a constant value of 400 nN for all the measurements. Each data point is an average of 15 nanoindentation measurements, and dashed lines are guides for the eyes. 50

Figure 3.4 Vibrational force constant κ (filled squares, ref 33), and the threshold ratio of contact radius to film thickness a/h (open squares), are plotted as a function of TMPC weight fraction, ϕ. Note that larger values of threshold a/h correspond to lower degree of substrate effect. 54

Figure 4.1 A SEM micrograph of the hemispherical AFM tip (radius, R ~ 550 nm) used in this study. 66

Figure 4.2 Typical FD curve obtain from an AFM nanoindentation measurement of h ~ 870 nm thick 64-arm SPS (M_n^{arm} = 9 kg/mol) film is shown: approach curve (open squares), retraction curve (open circles), and the JKR fitting (solid line). 68

Figure 4.3 (a) Effective moduli, $E(h)$, for LPS (M_w = 6 kg/mol), 8-arm SPS (M_n^{arm} = 14 kg/mol), and 64-arm SPS (M_n^{arm} = 9 kg/mol) films are plotted as a

function of film thickness, h. (b) $E(h)$ normalized with average effective moduli for $h > h_t$, E ($h > h_t$) are plotted as a function of ratio of contact radius to film thickness, a/h. Note that maximum force, F_{max}, was fixed at a constant value of 400 nN for all the nanoindentation measurements. Each data point is an average of 15 measurements, and dashed lines are guides for the eyes. 70

Figure A.1 Effective reduced moduli, $E_r(h)$, for (a) polystyrene and (b) tetramethyl bisphenol-A polycarbonate estimated by fitting force-distance curves with two different elastic contact models; the JKR (filled squares) and the DMT (open squares). The maximum force, F_{max}, was kept at a constant value of 400 nN for all the measurements. Each data point is an average of 15 nanoindentation measurements, and dashed lines are guides for the eyes……....81

List of Appendices

Appendix A 80

A.1 Analysis of nanoindentation data with the DMT model 80

A.2 References 81

Appendix B 82

B.1 Nanoindentation Experimental Procedure 82

B.2 Estimating effective modulus from force-distance curves 83

Abstract

This dissertation provides new and comprehensive insights into the nanoscale elastic mechanical response of supported polymer films. It is shown, using an atomic force microscopy nanoindentation technique, that thin polymer films supported by stiff (non-compliant) substrates exhibit effective elastic moduli E that increase with decreasing film thickness, h, for films thinner than a threshold film thickness h_t. The magnitude of h_t is a function of the polymer and its magnitude is typically in the range of a few hundred nanometers. A diverse range of polymer systems was investigated: (1) linear-chain polymers, (2) a miscible polymer/polymer blend system, and (3) star-shaped polymers.

For the case of linear-chain polymers, it is shown that indentation-induced stress field could be two orders of magnitude larger than the actual indentation depth, and the degree of enhancement of the effective modulus differs for different polymers. While h_t for polystyrene (PS) and poly(methyl methacrylate) (PMMA) films were comparable, h_t was smaller for polycarbonate (PC) films: h_t(PS) ~ h_t(PMMA) ~ 450 nm > h_t(PC) ~ 300 nm. In contrast to the current understanding of the field, it was shown that the elastic mechanical response of polymer films could not be fully understood in terms of the macroscopic modulus and Poisson's ratio of individual polymers and polymer/substrate interfacial interactions. We showed, for the first time, that this behavior is correlated with the local vibrational force constants (i.e. local stiffness), typically measured using incoherent neutron scattering, of the polymer films. The elastic mechanical response of a

miscible polymer/polymer blend was also rationalized in terms of the local elastic behavior of the blend, at different compositions, determined from incoherent neutron scattering measurements.

Finally, for the case of star-shaped PS molecules, the response was virtually identical to that of linear chain PS. However, h_t for a short arm star-shaped PS, with f = 64 arms, was nearly 50% larger. This is associated with the fact that the structure of the molecule is different; the molecules formed an ordered structure similar that that of particles or colloids.

Chapter 1

Introduction

1.1 Motivation and Research Objectives

In recent years, polymers have been developed for thin film applications such as membranes [1], sensors [2], and nanoimprinting [3]. Studies on thin polymer films have reported that the physical properties of polymer films exhibit film thickness dependencies. The glass transition temperature [4,5], structural relaxation [6], viscosity [7], and elastic modulus [8,9] of sufficiently thin polymer films have been shown to deviate from their bulk properties when film thickness is sufficiently thin. Such thickness dependent properties are known to be associated with changes in structure due to confinement and to interfacial interactions between polymer chain segments and external interfaces.

The mechanical properties of thin supported polymer films, in the nanoscale thickness range, are of interest in this dissertation. Mechanical properties of supported polymer films have been measured using thin film buckling [8,9] and Brillouin light scatter (BLS) measurements [10,11]. Thin film buckling experiments on polymer films reported that the elastic modulus of thin polymer films decreases with decreasing film thickness for thicknesses below 40~80 nm [8,9]. A bilayer model composed of a thin compliant surface layer and bulk-like layer was proposed to rationalize the decrease in

effective modulus with decreasing film thickness. Results from BLS measurements indicate that the high-frequency modulus is independent of film thickness for films as thin as ~40 nm [10,11]. Surface mechanical properties have been investigated using particle embedment experiments [12], and an evidence of compliant layer at the free surface was reported. However, these techniques are relatively indirect measurements and may not account for overall mechanical response of supported polymer films under deformation.

Nanoindentation techniques have been widely used to study mechanical properties of thin polymer films [13-19]. In contrast to thin film buckling and BLS measurements, nanoindentation techniques involve a direct contact between the tip and the surface of the sample. During nanoindentation measurements, indentation-induced stress field extends over a length scale of few hundreds of nanometers [13], and a mechanical response of a deformed layer on the same length scale is measured. However, measuring mechanical properties of polymer films supported by stiff substrates is challenging due to the effects associated with the underlying hard substrate. For polymer films supported on stiff substrates, increasing effective modulus with increasing indentation depth or decreasing film thickness has been reported; this is the so-called substrate effect [13-19]. When applied force is sufficiently large, or when film thickness is sufficiently thin, the indentation-induced stress field could extend throughout the entire film and strongly interact with the underlying stiff substrate [13]. As a result, an enhanced modulus compared to that of the bulk is observed. Thus, a systematic nanoindentation study on various thin polymeric films supported by stiff substrates would provide a deeper insight into understanding the effect of different chemical structures of

the polymers and different degree of polymer/interface interfacial interactions on the overall mechanical response of polymer films under confined geometry.

It was reported that the overall modulus of a thin polymer film could be influenced by interfacial interactions between polymer chains and underlying substrate [13]. By reconciling the finite element analysis predictions with the results from nanoindentation experiments, evidence of a modulus enhanced by strong attractive interfacial interactions at the polymer/substrate interface was reported. In contrast, a study on polymer films supported by two different substrates, one with strong and the other with weak interfacial interactions at the polymer/substrate interface, has reported that the geometrical confinement (i.e. presence of hard wall) may influence the mechanical properties more than such interfacial interactions [20]. Numerical studies on thin films have suggested that the substrate effect could be solely rationalized in terms of the macroscopic elastic moduli and Poisson's ratios of the film and the substrate [21-23]. Thus, the effect of polymer/substrate interfacial interactions on the overall mechanical properties is not well understood.

Apart from polymer/substrate interface, the mechanical properties near the free surface of polymer films are also not well understood. Nanoindentation studies on polymer films, moreover, have reported indentation depth dependent modulus at low indentation depths [13,15,17,24]. Specifically, the modulus has been shown to increase by a factor of up to 2 with decreasing indentation depths [15]. On the other hand, in a recent publication, it was reported that the strong enhancement of modulus near the free surface disappeared when nanoindentation experiments were performed in the linear

stress-strain regime and when adhesion between an indenter and the surface of a sample was properly taken into account [25].

Understanding the mechanical properties of thin polymer films on the length scale of tens to hundreds of nanometers is essential to design and develop new applications on the nanoscale. However, as described above, the mechanical properties of thin polymer films are controversial and still under debate to this date. Thus, for both academic interest and technical importance, a systematic study is strongly needed to understand and elucidate the factors influencing the overall mechanical properties of thin polymer films.

To this end, the objective of the research shown in this dissertation is to investigate the elastic mechanical response of different polymeric systems supported on stiff substrates. A thorough understanding of the factors influencing the mechanical response on the nanoscale will allow for a "*tailoring*" the mechanical properties of supported thin polymer films. The following sections of this Chapter will provide a brief background on the principle of atomic force microscopy (AFM) nanoindentation and the elastic contact mechanics model used in this study. And viability of the AFM nanoindentation technique will be followed.

1.2 Background

1.2.1 Principle of AFM Nanoindentation

Since the invention of AFM in 1986 [26], it has been widely used for the study of the mechanical properties of thin polymer films such as adhesion, friction, and mechanical modulus by means of force-distance (FD) curves [27]. Elastic or plastic properties are

examined by measuring deformation response of polymers under an externally applied force. Compared to nanoindenters which are also frequently used to examine mechanical properties of polymers, AFM has an advantage in term of force resolution which is up to two orders of magnitude higher than that of a nanoindenter.

AFM is designed to measure interaction forces between an AFM tip and the surface of sample. A schematic image of typical AFM components is shown in Figure 1.1. Vertical movement of an AFM probe which is composed of a tip and a cantilever is controlled by a z-piezo scanner, and lateral movement of sample stage is controlled by x- and y-piezo scanners. Laser beam is reflected on the back side of the cantilever, and the relative movement of the tip is recorded on a photodiode. During a nanoindentation measurement, the AFM tip vertically extents toward and retracts from the surface of sample, and a graph of Cantilever laser deflection, δ, versus Z-piezo displacement, Z, is recorded. This deflection-displacement curve can be converted into FD using the following equations [27].

$$D = Z - \delta \tag{1.1}$$

$$F = -k_c \delta \tag{1.2}$$

Distance, D, is simply the difference between displacement, Z, and deflection, δ, and force, F, is calculated using the Hooke's law by multiplying a known spring constant, k_c, and deflection, δ, of a cantilever. A FD curve is essentially a recording of interaction force between the tip and the surface of the sample as a function of relative distance of the tip normal to the surface.

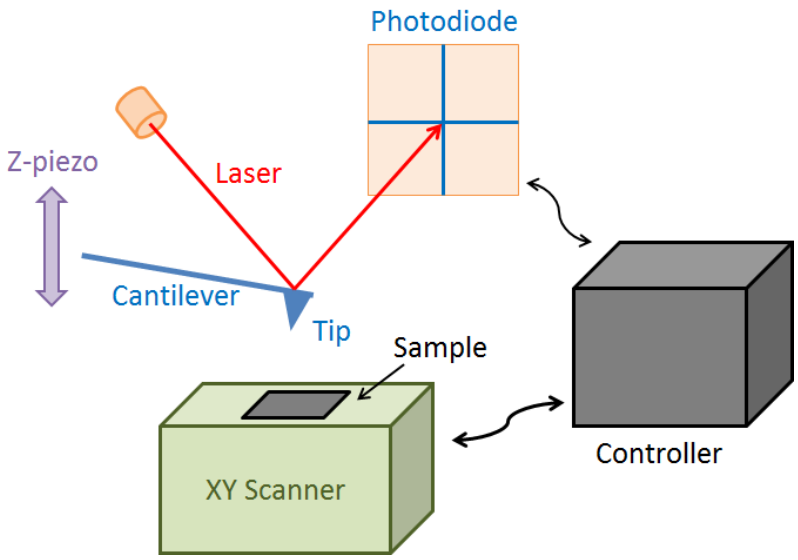

Figure 1.1 A schematic image of typical AFM components is shown.

A typical FD curve is shown in Figure 1.2, and it can be divided into different steps depending on the interaction between the AFM tip and the surface of the sample. First, the tip approaches toward the surface of the sample. Since the tip is sufficiently far away from the surface, it does not feel any interaction force and force remains zero. When the tip is close enough to the surface, attractive forces such as van der Waals force cause the tip to jump into the surface, and force becomes negative [27]. For soft polymeric materials, thus jump-in step may cause significant deformation even before the actual indentation step [27]. After proper contact between the tip and the surface of sample is established, the tip starts to indent the sample until it reaches the trigger force (maximum force). After the trigger force is reached, the tip starts to retract from the sample. Detachment between the tip and the surface occurs when maximum adhesion force (also known as pull-off force) is reached. When the tip moves far away from the surface, it does not feel any interaction force and force becomes zero again.

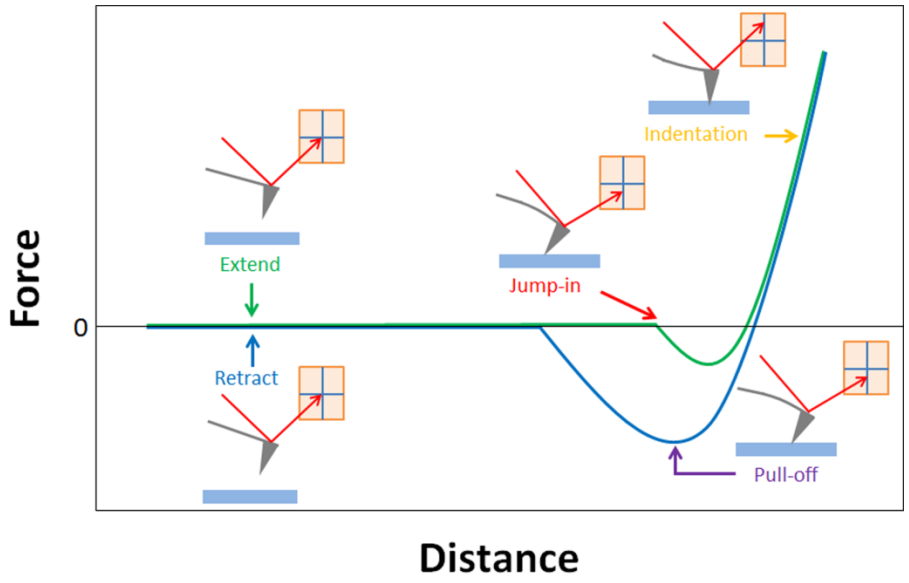

Figure 1.2 A schematic image showing different steps of a FD curve.

1.2.2 Elastic Contact Mechanics Models

The effective elastic moduli, *E*, of thin polymer films can be extracted from FD curves by fitting the curves with an appropriate elastic contact mechanics model. Typical models include the Hertz [28], Oliver-Pharr (OP) [29], Johnson-Kendall-Roberts (JKR) [30], and Derjaguin-Muller-Toporov (DMT) [31]. The Hertz, JKR, and DMT models are valid under conditions of elastic deformation [27]. While the Hertz model neglects effects due to the adhesion between the tip and sample surface, the other two models account for the effects of adhesion; the JKR model account for adhesion inside the contact area, and the DMT model account for adhesion outside the contact area [27]. On the other hand, the OP model, which estimates *E* from the initial slope of a retraction curve [29], is appropriate for conditions of elastic-plastic deformation. The OP model has been reported

to overestimate the modulus possibly due to plastic deformation and pile-up in the vicinity of the indentation center and to the viscoelasticity of polymers [32].

In case of the Hertz model, contact radius, *a*, and indentation depth, *d*, are estimated with the following equations [28]:

$$a = \left(\frac{R\,F}{K}\right)^{\frac{1}{3}} \tag{1.3}$$

$$d = \frac{a^2}{R} \tag{1.4}$$

where R is the radius of the tip, F is the externally applied force, K is the reduced modulus defined as $K = (4/3)E^*$. E^* is defined in terms of elastic modulus of the polymer, $E_{polymer}$, and the AFM tip, E_{tip}, and Poisson's ratio of the polymer, $\nu_{polymer}$, and the tip, ν_{tip}: $1/E^* = (1 - \nu_{polymer}^2)/E_{polymer} + (1 - \nu_{tip}^2)/E_{tip}$; since E_{tip} is much larger than $E_{polymer}$, it follows that $1/E^* \approx (1 - \nu_{polymer}^2)/E_{polymer}$ [33].

For the OP model, elastic modulus, *E*, is estimated using the following equation [29]:

$$E = \frac{(1-\nu_{polymer}^2)}{2\,\beta}\, S\, \frac{\sqrt{\pi}}{\sqrt{A}} \tag{1.5}$$

where β is an dimensionless correction parameter, S is the slope of early part of a FD curve during retraction, and A is the contact area between the tip and the surface of sample.

Both the JKR and DMT models are based on the Hertz model, but they account for effects associated with adhesion as mentioned above. The JKR model estimates contact radius, *a*, and indentation depth, *d*, with the following equations [30]:

$$a^3 = \frac{R}{K}[F + 3\pi WR + (6\pi FWR + (3\pi WR)^2)^{\frac{1}{2}}] \quad (1.6)$$

$$\mathrm{d} = \frac{a^2}{R} - \left(\frac{8\pi Wa}{3K}\right)^{\frac{1}{2}} \quad (1.7)$$

where *W* is the work of adhesion. According to the JKR model, *W* is defined in terms of maximum adhesion force, F_{ad}, and *R*: $W = -(2/3)(F_{ad}/\pi R)$. The DMT model estimates *a* and *d* with the following equations [31]:

$$a^3 = \frac{R}{K}[F + 2\pi WR] \quad (1.8)$$

$$\mathrm{d} = \frac{a^2}{R} = \frac{(F+2\pi RW)^{2/3}}{\sqrt[3]{RK^2}} \quad (1.9)$$

In case of the DMT model, *W* is defined such that $W = -(1/2)(F_{ad}/\pi R)$

1.3 **Viability of the AFM Nanoindentation Technique**

We performed a series of AFM nanoindentation experiments, based on the work of Dokukin and Sokolov, who discussed the viability of using different contact mechanics models to extract the elastic modulus *E* from a FD curve obtained using an AFM [25]. Dokukin and Sokolov employed Hertz, OP, JKR, and DMT models to fit same set of FD curves that were measured using a sharp tip (radius, $R \sim 22$ nm) and a hemispherical tip ($R > 810$ nm). For FD curves obtained with the sharp tip, regardless of which model was used for the analysis, an enhancement in *E* was observed for small

indentation depths. In contrast, the enhancement of E disappeared when FD curves were obtained using hemispherical tips and employing the JKR and DMT models, which accounted for the effects of adhesion between the tip and the sample surface. They concluded that the enhanced moduli at small indentation depths may originate from the nonlinearity of stress-strain relation (with the use of a sharp tip) and when the adhesion between the tip and sample surface is neglected from the analysis.

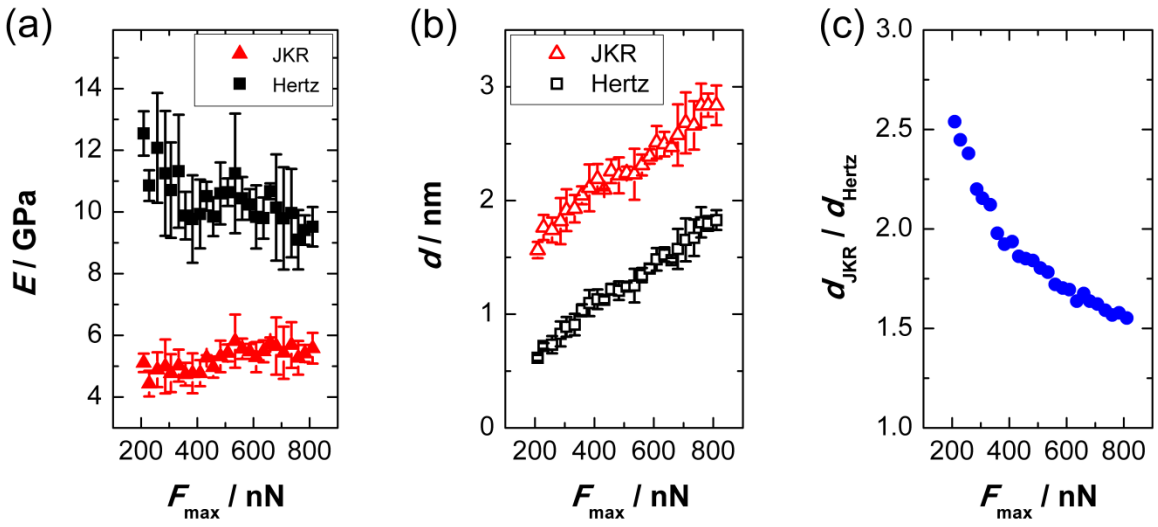

Figure 1.3 (a) Same set of FD curves was fitted with the Hertz model (filled squares) and JKR model (filled triangles) and the effective moduli, E, are plotted as a function of maximum force, F_{max}. Each data point is an average of 3 nanoindentation measurements. (b) The corresponding indentation depths, d, from data shown in part (a) are plotted with open symbols as a function of F_{max}. Each data point is an average of 3 nanoindentation measurements. (c) The relative underestimation of d (ratio of d estimated by the JKR and Hertz models) is shown as a function of F_{max}.

We performed AFM nanoindentation measurements on a ~1 μm thick polystyrene film, supported by oxidized silicon substrate, using different maximum forces, F_{max}, from 200 nN to 800 nN. The Hertz and JKR models were used to extract E from a same set of FD curves and results are shown in Figure 1.3a. When the Hertz model, which neglects

the effects of adhesion between the tip and film surface [38], was used to fit the FD curve, the estimated E increased with decreasing F_{max} or indentation depth, d. In contrast, only a slight increment of the moduli was observed with increasing F_{max} when the analysis was performed using the JKR model, which accounts for the effects of adhesion [38]. This slight increase in E with increasing F_{max} can be attributed to effects associated with the underlying stiff substrate; the stress field created under indentation propagates further into the film with increasing F_{max}. The enhancement in E is observed due to increasing interactions between the stress field and underlying substrate (the "substrate effect") [11]. Indentation depths estimated using the JKR model (d_{JKR}) and the Hertz model (d_{Hertz}) are plotted as a function of F_{max} in Figure 1.3b and it is shown that the Hertz model underestimates indentation depths compared to those estimated by the JKR model. The relative underestimation of indentation depth (d_{JKR}/ d_{Hertz}), plotted in Figure 1.3c, reveals that the relative underestimation is larger for lower values of F_{max}; the extent of the underestimation decreases with increasing F_{max}. It is important to point out that the dependence of d_{JKR}/d_{Hertz} on F_{max} exhibits a trend similar to the enhancement of the moduli shown in Figure 1.3a. This suggests that the increasing E with decreasing F_{max} (Figure 1.3a) originates from an underestimation of the indentation depth with decreasing F_{max} (Figure 1.3c). Our observations are in agreement with those of Dokukin and Sokolov [22]. Therefore, we used the JKR model for the analysis of the indentation data in our study.

1.4 References

1. Rowe, B. W.; Freeman, B. D.; Paul, D. R. Physical aging of ultrathin glassy polymer films tracked by gas permeability. *Polymer* **2009,** *50*, 5565-5575.

2. Lee, D.; Jung, J.; Bilby, D.; Kwon, M. S.; Yun, J.; Kim, J. A novel optical ozone sensor based on purely organic phosphor. *ACS Appl. Mater. Interfaces* **2015,** *7*, 2993-7.

3. Pina-Hernandez, C.; Kim, J. S.; Guo, L. J.; Fu, P. F. High-throughput and etch-selective nanoimprinting and stamping based on fast-thermal-curing poly(dimethylsiloxane)s. *Adv. Mater.* **2007,** *19*, 1222-1227.

4. Keddie, J. L.; Jones, R. A. L.; Cory, R. A. Size-dependent depression of the glass-transition temperature in polymer-films. *Europhys. Lett.* **1994,** *27*, 59-64.

5. Keddie, J. L.; Jones, R. A. L.; Cory, R. A. Interface and surface effects on the glass-transition temperature in thin polymer-films. *Faraday Discuss.* **1994,** *98*, 219-230.

6. Priestley, R. D. Physical aging of confined glasses. *Soft Matter* **2009,** *5*, 919-926.

7. Masson, J. L.; Green, P. F. Viscosity of entangled polystyrene thin film melts: Film thickness dependence. *Phys. Rev. E* **2002,** *65*, 031806.

8. Stafford, C. M.; Vogt, B. D.; Harrison, C.; Julthongpiput, D.; Huang, R. Elastic moduli of ultrathin amorphous polymer films. *Macromolecules* **2006,** *39*, 5095-5099.

9. Torres, J. M.; Stafford, C. M.; Vogt, B. D. Elastic modulus of amorphous polymer thin films: relationship to the glass transition temperature. *ACS Nano* **2009,** *3*, 2677-2685.

10. Sun, L.; Dutcher, J. R.; Giovannini, L.; Nizzoli, F.; Stevens, J. R.; Ord, J. L. Elastic and elasto-optic properties of thin-films of poly(styrene) spin-coated onto Si(001). *J. Appl. Phys.* **1994,** *75*, 7482-7488.

11. Cheng, W.; Sainidou, R.; Burgardt, P.; Stefanou, N.; Kiyanova, A.; Efremov, M.; Fytas, G.; Nealey, P. F. Elastic properties and glass transition of supported polymer thin films. *Macromolecules* **2007,** *40*, 7283-7290.

12. Karim, T. B.; McKenna, G. B. Evidence of surface softening in polymers and their nanocomposites as determined by spontaneous particle embedment. *Polymer* **2011,** *52*, 6134-6145.

13. Watcharotone, S.; Wood, C. D.; Friedrich, R.; Chen, X. Q.; Qiao, R.; Putz, K.; Brinson, L. C. Interfacial and substrate effects on local elastic properties of polymers using coupled experiments and modeling of nanoindentation. *Adv. Eng. Mater.* **2011,** *13*, 400-404.

14. Domke, J.; Radmacher, M. Measuring the elastic properties of thin polymer films with the atomic force microscope. *Langmuir* **1998,** *14*, 3320-3325.

15. Tweedie, C. A.; Constantinides, G.; Lehman, K. E.; Brill, D. J.; Blackman, G. S.; Van Vliet, K. J. Enhanced stiffness of amorphous polymer surfaces under confinement of localized contact loads. *Adv. Mater.* **2007,** *19*, 2540-2546.

16. Silbernagl, D.; Cappella, B. Mechanical properties of thin polymer films on stiff substrates. *Scanning* **2010,** *32*, 282-293.

17. Xu, W.; Chahine, N.; Sulchek, T. Extreme hardening of PDMS thin films due to high compressive strain and confined thickness. *Langmuir* **2011,** *27*, 8470-8477.

18. Geng, K. B.; Yang, F. Q.; Druffel, T.; Grulke, E. A. Nanoindentation behavior of ultrathin polymeric films. *Polymer* **2005,** *46*, 11768-11772.

19. Zhou, J.; Komvopoulos, K. Surface and interface viscoelastic behaviors of thin polymer films investigated by nanoindentation. *J. Appl. Phys.* **2006,** *100*, 114329.

20. Cheng, X.; Putz, K. W.; Wood, C. D.; Brinson, L. C. Characterization of local elastic modulus in confined polymer films via AFM indentation. *Macromol. Rapid Comm.* **2015,** *36*, 391-397.

21. Perriot, A.; Barthel, E. Elastic contact to a coated half-space: Effective elastic modulus and real penetration. *J. Mater. Res.* **2004,** *19*, 600-608.

22. Clifford, C. A.; Seah, M. P. Modelling of nanomechanical nanoindentation measurements using an AFM or nanoindenter for compliant layers on stiffer substrates. *Nanotechnology* **2006,** *17*, 5283-5292.

23. Clifford, C. A.; Seah, M. P. Nanoindentation measurement of Young's modulus for compliant layers on stiffer substrates including the effect of Poisson's ratios. *Nanotechnology* **2009,** *20*, 145708.

24. Briscoe, B. J.; Fiori, L.; Pelillo, E. Nano-indentation of polymeric surfaces. *J. Phys.D Appl. Phys.* **1998,** *31*, 2395-2405.

25. Dokukin, M. E.; Sokolov, I. On the Measurements of Rigidity Modulus of Soft Materials in Nanoindentation Experiments at Small Depth. *Macromolecules* **2012,** *45*, 4277-4288.

26. Binnig, G.; Quate, C. F.; Gerber, C. Atomic force microscope. *Phys. Rev. Lett.* **1986,** *56*, 930-933.

27. Butt, H. J.; Cappella, B.; Kappl, M. Force measurements with the atomic force microscope: Technique, interpretation and applications. *Surf. Sci. Rep.* **2005,** *59*, 1-152.

28. Johnson, K. L. *Contact mechanics*; Cambridge University Press: Cambridge Cambridgeshire ; New York, 1985.

29. Oliver, W. C.; Pharr, G. M. Measurement of hardness and elastic modulus by instrumented indentation : Advances in understanding and refinements to methodology. *J. Mater. Res.* **2004,** *19*, 3-20.

30. Johnson, K. L.; Kendall, K.; Roberts, A. D. Surface energy and contact of elastic solids. *Proc. R. Soc. Lon. Ser-A* **1971,** *324*, 301-313.

31. Derjaguin, B. V.; Muller, V. M.; Toporov, Y. P. Effect of contact deformations on adhesion of particles. *J. Colloid Interf. Sci.* **1975,** *53*, 314-326.

32. Tranchida, D.; Piccarolo, S.; Loos, J.; Alexeev, A. Mechanical characterization of polymers on a nanometer scale through nanoindentation. A study on pile-up and viscoelasticity. *Macromolecules* **2007,** *40*, 1259-1267.

33. Passeri, D.; Rossi, M.; Tamburri, E.; Terranova, M. L. Mechanical characterization of polymeric thin films by atomic force microscopy based techniques. *Anal. Bioanal. Chem.* **2013,** *405*, 1463-1478.

Chapter 2

The Elastic Mechanical Response of Supported Thin Polymer Films

2.1 Introduction

The mechanical properties of thin polymer films are of scientific and technological interest to diverse communities of researchers. This interest is partly driven by applications that range from thin film devices and sensors to active and passive coatings and flexible displays [1,2]. The physical properties, from transport and relaxation processes to phase stability and glass transition temperature, T_g, of macromolecular thin film systems with thicknesses, h, in the range of nanometers to several tens of nanometers, are typically thickness dependent [3-11]. Thickness dependent properties arise fundamentally in part from entropic effects, associated with confinement, and enthalpic intermolecular effects, which influence the long and short-range structure and properties of the polymer.

Nanoindentation techniques have been widely used to extract the mechanical properties of different polymers [12-20]. It is well accepted that the mechanical properties of a supported thin polymer could be affected by the underlying substrate. Indentation experiments have shown that the effective modulus of a thin polymer film supported by a stiff substrate increases with decreasing film thickness (over a thickness range of a few hundred nanometers) or with increasing applied force (hence increasing indentation depth, d) due to effects associated with the underlying hard substrate; this is the so-called "substrate effect" [21-28]. It has been shown that the stress field would impinge and interact with the substrate, leading to an enhanced mechanical modulus, for films in the thickness range of a few hundred nanometers [27].

Several numerical studies of supported thin films have been performed to evaluate and to understand the "substrate effect" [29-31]. For systems composed of a soft film on a stiff substrate, it has been shown that for small values of the ratio of contact radius to film thickness, a/h, the estimated reduced modulus of the system is similar to that of the film [29]. However, with increasing a/h, the substrate effect becomes significant and the reduced modulus of the system approaches that of the substrate. The onset of the transition from a bulklike to a substratelike mechanical response shifts to greater values of a/h with increasing mismatch between the reduced moduli of the soft film and stiff substrate. Clifford and Seah have shown that the normalized reduce moduli curves are superimposable when plotted as a function of $a/h(E_L^*/E_S^*)^{0.63}$, where E_L^* and E_S^* are the reduced modulus of the film and substrate, respectively [30]. For conditions under which $E_L^*/E_S^* = 0.1$, a stronger substrate effect was observed with increasing Poisson's ratio of the film [31]. These results suggest that the enhanced moduli of thin supported films

compared to the bulk, that is, the substrate effect, could be rationalized in terms of the elastic moduli and Poisson's ratios of the components, that is, film and substrate.

In a recent publication, Watcharotone et al. showed that, in addition to "substrate effect," the magnitude of the effective mechanical modulus might also be sensitive to the interfacial interactions between the polymer and the substrate [27]. They performed nanoindentation experiments on poly(methyl methacrylate) (PMMA) films supported on oxidized silicon substrates, SiO_x; strong specific interactions (hydrogen bonding) between the PMMA and the SiO_x substrate are known to influence physical properties, leading to an h-dependent T_g, of the PMMA [32]. Watcharotone et al. observed evidence of an interface layer in the vicinity of the substrate with the modulus at least twice that of the bulk by numerically subtracting the finite element analysis (FEA) results from experimental results. These results suggest an additional interaction, known to influence the physical properties of thin polymer films, needs to be considered.

Based on the foregoing, natural questions would be associated with the role of the polymer substrate interaction and the structure of the polymer on the overall mechanical response. To this end, an experimental study that systematically considers polymers of varying chemical structures and local chain stiffness, which are known to be important with regard to bulk deformation mechanisms of polymers, and varying polymer/substrate interactions would provide additional insights into possible processes that significantly contribute to the mechanical response of thin supported polymer films. Nanoindentation measurements were performed, using atomic force microscopy (AFM), on poly(methyl methacrylate) (PMMA), polystyrene (PS), polycarbonate (PC), and poly(vinyl chloride) (PVC) films supported on oxidized silicon substrates. The "substrate effect" was found to

be comparable for PMMA and PS films supported by SiO_x substrates; these were appreciably larger than those for PVC and PC. FEA results show that our experimental results cannot be rationalized solely in terms of the moduli and Poisson's ratios of the constituents (polymer and substrate) of the system. Contributions associated with molecular characteristics of the polymer (i.e.: chain stiffness and related differences in the local vibrational force constant, manifested in the mean-square atomic displacements of the polymer) need to be considered in order to gain appropriate insight into the mechanical response of thin supported polymer films.

2.2 Experimental Section

2.2.1 Sample Preparation

Thin polymer films were prepared by spin coating solutions of each polymer onto oxidized (~1.7 nm native oxide layer) silicon substrates (Wafer World). Solutions of PS (Pressure Chemical, M_w = 130 kg/mol, M_w/M_n = 1.06) and PMMA (Polymer Source, M_w = 151 kg/mol, M_w/M_n = 1.09) were prepared using toluene as the solvent, and solutions of PC (Acros Organics, M_w = 64 kg/mol) and PVC (Polymer Standard Service, M_w = 73 kg/mol, M_w/M_n = 1.12) were prepared using cyclohexanone as the solvent. Each film was subsequently annealed under vacuum at a temperature of 20 ℃ above the bulk T_g of the polymer for more than 12 h in order to remove residual solvent. Film thicknesses, which varied from 1 μm to 200 nm, were measured using spectroscopic ellipsometry (JA Woolam, M-2000).

2.2.2 Atomic Force Microscope

The nanoindentation experiments were performed using an atomic force microscope (Asylum Research, MFP-3D), with a hemispherical AFM tip, at a temperature, *T*, of 30 ℃, under closed loop mode, in order to maintain a constant indentation rate of 30 nm/s. Hemispherical AFM tips (radius, $R \sim 570$ nm) were prepared by annealing AFM probes (NanoWorld, NCH) in air for ∼4 h at 1200 ℃ [16]. The tip was examined prior to and after nanoindentation measurements using a scanning electron microscope (FEI, Nova Nanolab 200) to ensure that the shape and dimension did not change during measurements. The sensitivity of the AFM cantilevers were calibrated on a freshly cleaved mica substrate, and the spring constants, measured by thermal tune method [33], were approximately 29 N/m. The surface root-mean-square (RMS) roughness of the polymer films, measured over the surface area of 5×5 μm^2, was 0.28 nm on average.

2.2.3 Elastic Contact Mechanical Model

The Johnson-Kendall-Roberts (JKR) model which was used to extract *E* from FD curves predicts that the indentation depth is a function of the radius of contact between the indenter and sample surface, *a*, the applied force, *F*, the radius of the indenter, *R*, the work of adhesion, *W*, and the reduced modulus ($K = (4/3)E^*$) [19]:

$$a^3 = \frac{R}{K}\left[F + 3\,\pi\,R\,W + \left(6\,\pi\,R\,W\,F + (3\,\pi\,R\,W)^2\right)^{\frac{1}{2}}\right] \quad (2.1)$$

$$d = \frac{a^2}{R} - \left(\frac{8\,\pi\,W\,a}{3K}\right)^{\frac{1}{2}} \quad (2.2)$$

E^* is defined in terms of elastic modulus of the polymer, $E_{polymer}$, and of the AFM tip, E_{tip}, and Poisson's ratio of the polymer, $\nu_{polymer}$, and of the tip, ν_{tip}: $1/E^* = (1 - \nu_{polymer}^2) / E_{polymer} + (1 - \nu_{tip}^2) / E_{tip}$; since $E_{tip} \gg E_{polymer}$, it follows that $1/E^* \approx (1 - \nu_{polymer}^2) / E_{polymer}$ [20]. According to the JKR model, W is defined such that $W = -2/3(F_{ad}/\pi R)$, where F_{ad} is maximum adhesion force (or pull-off force) [34]. Poisson's ratios of $\nu = 0.33$ for PS and PMMA [35], 0.37 for PC [36], and 0.38 for PVC were used [37].

2.2.4 Finite Element Analysis

Nanoindentation experiments on thin films were simulated using the simulation software (SIMULIA, Abaqus 6.12). The axisymmetric model used in this study was composed of two parts: one was an analytical rigid spherical indenter with a 570 nm radius and the other was a deformable film with different h from 1 μm to 200 nm. The deformable film was modeled assuming elastic behavior and nonstructured 8-node biquadratic axisymmetric quadrilateral (CAX-8) elements were used with a global size of 1×10^{-5} and tangential friction coefficient of 0.1. A rigid boundary condition was applied to the film/substrate interface to simulate the effects of a hard supporting substrate. Identical maximum force, $F_{max} = 400$ nN, with experiments was applied in the simulation and all simulation parts were modeled with their exact dimensions. It should be noted that the adhesion between the indenter and film surface was assumed to be zero for simplicity and hence the Hertz model was applied to fit FD curves obtained by the simulation [19].

2.3 **Results and Discussion**

The mechanical responses of a series of films composed of PMMA, PS, PC, and PVC with different thicknesses were studied using AFM nanoindentation measurements. A typical force-distance (FD) curve is shown in Figure 2.1: approach (curve represented by open squares) and retraction (curve represented by open circles). When the AFM tip is sufficiently close to the surface of the film, the tip abruptly impinges the surface of the film, likely due to attractive van der Waals forces [19]. After reaching the maximum applied force, F_{max}, the tip retracts and the detachment between the tip and film surface occurs at the so-called pull-off force.

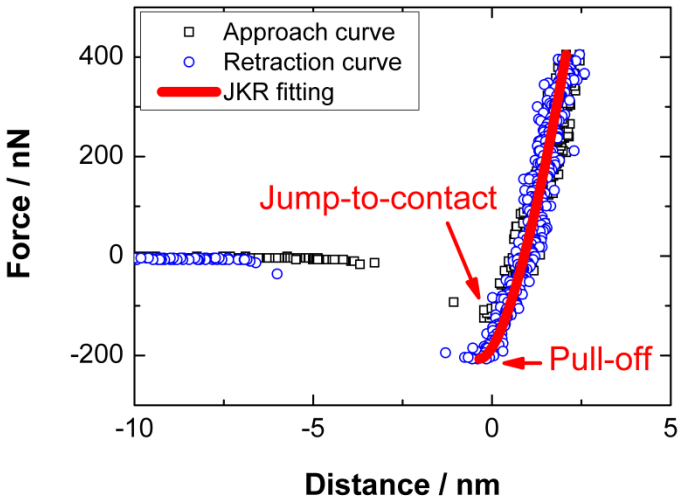

Figure 2.1 Typical FD curve obtained from an AFM nanoindentation measurement on $h \sim 1$ μm PS film fitted with the JKR model: approach curve (open squares), retraction curve (open circles), and the JKR fitting (solid line). Note that the approach and retraction curves overlap without hysteresis, indicating the deformation behavior is purely elastic.

We note that the approach and retraction curves in Figure 2.1 overlap, revealing the absence of hysteresis in the contact regime; this indicates that the deformation during

indentation was purely elastic, not plastic [19]. The effective modulus, E, was estimated by fitting the entire retraction curve using the JKR model [14]. In order to check for possible viscoelastic effects on the measurements, nanoindentation measurements were performed at different indentation rates (from 30 to 120 nm/s) on $h \sim 1$ μm films and the E was independent of indentation rate, indicating the absence of the influence of viscoelastic effects on the measurement of the modulus. This is not surprising, considering the indentation rates and the fact that the measurements were performed at T = 30 ℃, which is well below the T_g's of all polymers used in our study. We performed nanoindentation measurements of a bare silicon substrate, and there was no evidence of deformation for forces F_{max} = 1 μN, which indicates that the substrate may be considered to be nondeformable during measurements.

The moduli $E(h)$ are plotted for PMMA, PS, PC, and PVC films in Figure 2.2a, as a function of h for thicknesses ranging from 200 nm to 1 μm. For these measurements, F_{max} was kept at a constant value of 400 nN. For PMMA, PS, and PC films, $E(h)$ increases with decreasing h for h less than a threshold thickness, h_t, whereas for PVC films $E(h)$ is independent of h. Note that the same value of F_{max} was used in all these experiments. The h_t is comparable for PMMA and PS ($h_t \sim 450$ nm) but smaller for PC ($h_t \sim 300$ nm): h_t(PMMA) ~ h_t(PS) > h_t(PC). The extent of the substrate effect may be compared by plotting E as a function of a/h or d/h [26,27,29]. The $E(h)$ data from Figure 2.2a are normalized with the average effective moduli for $h > h_t$, $E(h > h_t)$, and are plotted as a function of a/h in Figure 2.2b. Like to the trends shown in Figure 2.2a, PMMA and PS films exhibit a very similar mechanical response, showing largest degree of enhancement of the different polymers studied. While $E(h)/E(h > h_t)$ of PVC films are

relatively independent for values of a/h used, those of PC films increase at higher values of a/h compared to those of PMMA and PS films. We should emphasize here that our experiments are performed in the elastic deformation regime. At sufficiently larger strains, these polymers would undergo plastic deformation and the mechanisms of plastic deformation of these polymers are different. This issue is not of interest in our study.

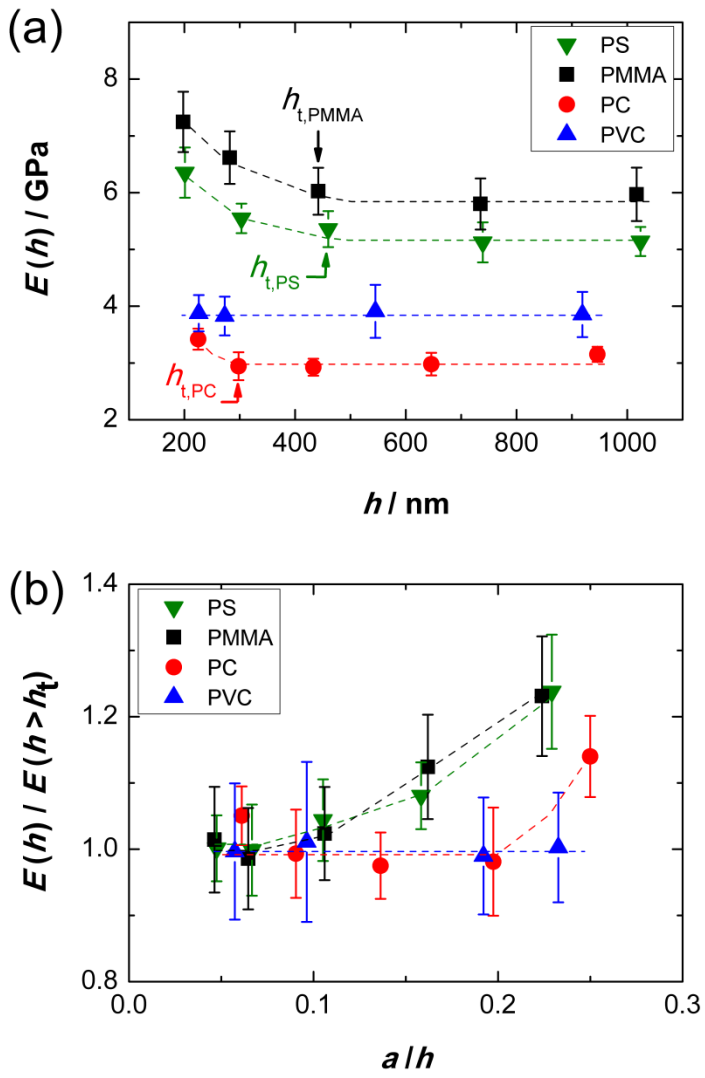

Figure 2.2 (a) Effective moduli, $E(h)$, measured for PMMA, PS, PC, and PVC films at fixed maximum force, F_{max}, of 400 nN plotted as a function of film thickness, h; dashed lines are guides for the eyes. (b) $E(h)$ normalized with average effective moduli for $h > h_t$, $E(h > h_t)$, and plotted as a function of ratio of contact radius to film thickness, a/h. Each data point is an average of 10 nanoindentation measurements, and dashed lines are guides for the eyes.

As mentioned above, the enhancement of E for thin polymer films supported by stiff substrates has been discussed in terms of substrate effect [21-28]. When a polymer film is thinner than h_t, the indentation-induced stress field interacts significantly with the stiff supporting substrate leading to enhanced moduli. It was suggested, and briefly

mentioned above, that the polymer/substrate interactions can also affect the mechanical response of supported films [27]. Specifically, for the PMMA/SiO_x system, the enhancement of moduli may partly be due to the presence of a layer in the vicinity of the substrate with enhanced moduli compared to the bulk. This layer was suggested to be due to strong attractive interactions between PMMA segments and the oxidized layer. However, our studies reveal that the magnitudes of the substrate effect for PMMA/SiO_x and PS/SiO_x are comparable for both systems. This is noteworthy because PMMA/SiO_x interfacial interactions are highly specific, whereas PS has nonwetting interactions with SiOx interface [9,32]. These results suggest that the effects associated with polymer/substrate interactions are not significant in nanoindentation experiments. In fact, strong bonding at an interface would enhance the local density profile of the polymer on a length scale of nanometers (see refs 3 or 4, for example). This would in principle increase the local modulus on the same length scales. This would be the reason that substrate/polymer interactions would not be significant for measurements of films with thicknesses on the order of tens or hundreds of nanometers.

It would be appropriate to comment on the role of the other interface, the free surface, on the mechanical response. The free surface of a polymer film has been suggested, based on particle embedment experiments where adhesion between a particle and sample surface is the only driving force, to be softer than the bulk [38,39]. In addition, the T_g of the free surface of a linear-chain polymer film is known to be lower than the bulk due to the enhanced configurational freedom of polymer chains in the vicinity of the free surface [9,40]. Therefore, one may anticipate a lower E near the free surface. However, evidence of soft surface layer was not detected in our indentation

experiments. This is not unexpected for the following reasons. In indentation experiments, where an external force, F_{max}, is applied, the indentation-induced stress field propagates much deeper into a film compared to the indentation depth and the actual probing volume may be much larger than one may expect [15,30,31]. The magnitude of propagation, shown by h_t in Figure 2.2a, is on the order of several hundreds of nanometers even for indentation depths of few nanometers. Hence, the estimated $E(h)$ is not a measure of the mechanical response of the thin surface layer (length scales of nanometers), but rather it is the response of an entire film of thickness h, where h is hundreds of nanometers.

To further investigate the substrate effect, additional nanoindentation measurements were performed on PMMA, PC, and PVC films with similar thicknesses, $h \sim 320$ nm, using values of the applied force F_{max} that varied from 300 to 700 nN. The estimated E are plotted as a function of F_{max} in Figure 2.3. The magnitude of substrate effect would be expected to increase with increasing force or indentation depth as the induced stress field further propagates into films and strongly interacts with the underlying substrate [27]. However, the degree of enhancement significantly differed between different polymers. E of the PMMA film exhibits the strongest dependence on F_{max} while the PVC film showed a reasonably independent dependence on F_{max}. The PC film showed a weaker dependence on F_{max} compared to that of the PMMA film.

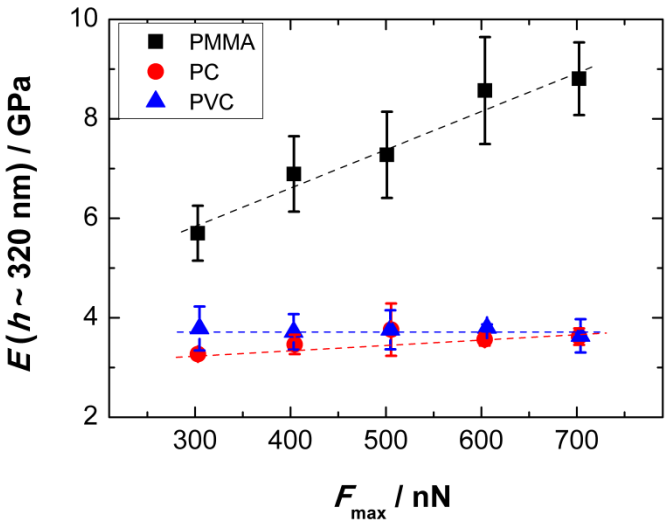

Figure 2.3 Effective moduli, E, measured for PMMA, PC, and PVC films with similar film thickness, $h \sim 320$ nm, as a function of F_{max} from 300 nN up to 700 nN. Each data point is an average of three nanoindentation measurements, and dashed lines are guides for the eyes.

We used FEA to simulate the mechanical response of supported films for indentation conditions such that a/h was small, corresponding to our experiments (Figure 2.2) [27,29-31]. Perriot and Barthel [29] addresses the questions of a wide range of much larger values of a/h, not of interest in our study. We simulated conditions under which F_{max} was fixed at 400 nN. Elastic moduli (taken from our experimental results) of E = 5.9 GPa for PMMA, 5.2 GPa for PS, 3.0 GPa for PC, and 3.9 GPa for PVC and Poisson's ratios of ν = 0.33 for PMMA and PS [35], 0.37 for PC [36], and 0.38 for PVC were used [37]. These input values mimicked conditions under which the mechanical properties of films are relevant to the polymers we studied. In Figure 2.4, the effective moduli, normalized with elastic modulus of the film, $E_{polymer}$, are plotted as a function of a/h. The enhancement of $E(h)/E_{polymer}$ is due to the substrate effect, that is, propagation of the stress field and interaction with the underlying stiff substrate (insets in Figure 2.4) [27].

Regardless of differences between the elastic moduli and Poisson's ratios of the simulated films, the curves overlay reasonably well and differences in the substrate effects are virtually indistinguishable. Based on the data in Figure 2.2b and Figure 2.4, it is clear that FEA fails to account for actual elastic response of different polymeric materials. We attribute this inconsistency to the fact that the homogeneous solid model used in FEA does not account for microstructural information such as chemical structure, specific volume, and local chain stiffness of different polymers [41-43]. Note that simulated stress fields from FEA (insets in Figure 2.4) show that the stress field extends over several hundreds of nanometers into the film even for indentation depths $d < 2$ nm. This also indicates that the actual probing depth is much deeper than the indentation depth [15,30,31].

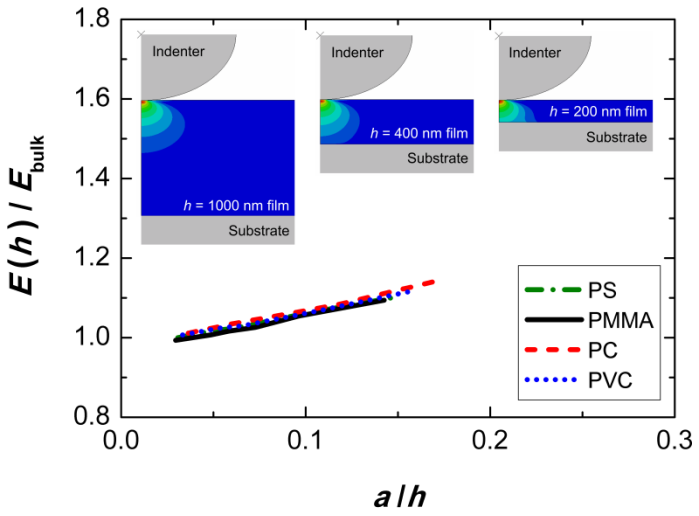

Figure 2.4 Simulated normalized effective moduli, $E(h)/E_{polymer}$, are plotted as a function of a/h. $E_{polymer}$ were taken from our experimental results (E_{PMMA} = 5.9 GPa, E_{PS} = 5.2 GPa, E_{PC} = 3.0 GPa, and E_{PVC} = 3.9 GPa) and Poisson's ratios were taken from the literature ($\nu_{PMMA} = \nu_{PS} = 0.33$, $\nu_{PC} = 0.37$, and $\nu_{PVC} = 0.38$). Note that the moduli curves almost overlay regardless of differences in the elastic modulus and Poisson's ratio of the simulated films. Insets show the indentation-induced stress field under the indentation center for h = 1000 nm, h = 400 nm, and h = 200 nm films (from left to right) for simulated PMMA films. Meshes are not shown for visual clarity.

We now discuss potential reasons for the different a/h dependences of the moduli exhibited by the polymer films studied in this work. The data in Figure 2.2 indicate that, for a given a/h, propagation of the stress field may be larger for PMMA and PS compared to PC and PVC. The mechanical properties of PC and PVC are known to be different from those of PS and PMMA. The mechanisms and extent of failure, though not specifically relevant here, are different for each polymer [43]; the impact strength of PC and PVC is known to be much higher than those of PMMS and PS [44]. Nevertheless, one could argue that these differences may in part be associated with the magnitude of the propagation of the stress field in the polymers under applied external forces. Of course, we reiterate that these considerations refer to the behavior of the materials under conditions of high strain and not in the elastic regime.

Considering that we are concerned with the elastic response of the materials, an important consideration would be the thermal mean square displacement, vibrations of atoms in a solid, which provide insight into the phonon modes and the local elasticity of the material. The amplitude of thermal vibrations of atoms in polymers has been measured via incoherent neutron scattering (INS) experiments [45-47]. It was found that, for sufficiently low T, the mean-square displacement of atoms ($\langle u^2 \rangle$) increases linearly with T due to harmonic oscillations, $\langle u^2 \rangle \sim k_b T/\kappa$ (where k_b is the Boltzmann constant and κ is the vibrational force constant). In this linear regime, larger values of κ are associated with smaller values of $\langle u^2 \rangle$. For higher T, $\langle u^2 \rangle$ increases more rapidly due to anharmonic motions. Experimentally, it has been reported that the force constant for PVC and PC are higher than that of PMMA: $\kappa_{PVC} \sim 2\kappa_{PC} \sim 4\kappa_{PMMA}$ [42].

We found an interesting correlation between the effect of the substrate on E and the magnitude of κ for the PMMA, PC, and PVC films. Recall that the effect of substrate on the moduli for PMMA films was observed at higher film thicknesses ($h_t \sim 450$ nm) compared to PC films which occurred at lower film thicknesses ($h_t \sim 300$ nm); an enhancement of the moduli was not observed for PVC films in the thickness range we studied. If the mean square displacement of atoms in polymer A is naturally larger than those in polymer B at a given T, for a given a/h, it is probable that the propagation of the deformation-induced stress field would be larger in polymer A compared to the propagation in polymer B. This suggests that the indentation-induced stress field may propagate further into PMMA films due to smaller value of κ (i.e. lower local elasticity of polymer chains) compared to those of PC and PVC for a given a/h. In effect, we are suggesting that a viable argument may be made that the thickness dependence of the effective modulus of polymer thin films reported in this study is an intrinsic property associated with $<u^2>$, and hence the local stiffness, κ, of the material. For smaller values of κ, the stress field propagates further into the film and the effects of the underlying substrate become more apparent than in systems in which κ is larger.

Recent theory and simulations establish the connection between dynamics and the elastic mechanical response of polymers [48]. This connection is based on an extension of the mesoscale "percolation of free volume distribution" (PFVD) model, proposed by Dequidt et al. The notion is that the materials response, in the vicinity of T_g and at lower T, is characterized by a glassy modulus and a viscous modulus [49,50]. High-frequency relaxations would be associated with the glassy modulus and low frequency fluctuations would be associated with the viscous modulus. Parenthetically, the PFVD model is based

on a well accepted concept that the dynamics of liquids are heterogeneous, characterized by local regions of dimensions ξ, on the order of nanometers, that relax at different rates, some very fast compared to the average and others slow compared to the average. These domains are the result of local density fluctuations. Fluctuations of the domains and interactions between them are responsible for the frequency response, over a range of high and low frequencies, that characterize the behavior of materials, and hence the mechanical response, over all temperatures. It should be further noted that simulations by Riggleman et al. show that, for temperatures $T < T_g$, the structure of a glassy solid is characterized by a local elasticity map [51]. The elasticity varies on length scale of nanometers. An assessment of the local elasticity is accomplished through the measurement of the mean-square-displacement using INS, as discussed above.

2.4 **Conclusion**

In conclusion, we investigated the effective moduli, E, of thin PMMA, PS, PC, and PVC films supported by SiO_x substrates, using AFM nanoindentation, as a function of film thickness, h, and the ratio of contact radius to film thickness, a/h. We show that the threshold thickness, h_t, where E starts to increase with decreasing h, depends primarily on the chemical structures and local chain stiffness of the polymers. The threshold thickness h_t is comparable for PMMA and PS films, but this thickness is larger than that for PC films. In other words, the normalized moduli, $E(h)/E(h > h_t)$, increases at lower a/h values for PMMA and PS films compared to PC films. For PVC films, the moduli and normalized moduli were fairly independent of h and a/h, respectively. While the FEA measurements are useful, they do not fully explain the response of polymers of varying

chemistries. Our results strongly indicate that the mechanical response of the polymers cannot only be understood in terms of the individual moduli and Poisson's ratios, of the polymer and substrate, as suggested by FEA. Moreover, the nature of the polymer-substrate interactions, which are generally known to influence the physical properties of polymer thin films, do not provide a satisfactory rationalization of the mechanical response. Our results suggest that, in order to better understand the differing elastic deformation behaviors of thin supported polymer films, atomistic/molecular information associated with the mean square atomic displacements, as measured using incoherent neutron scattering, and hence the local stiffness, κ, need to be considered. Molecular simulations, which could account for the chemistry and various intrinsic and extrinsic intermolecular interactions, are required to fully understand the elastic mechanical response of thin supported polymer films.

2.5 References

1. Sakai, Y.; Sadaoka, Y.; Matsuguchi, M. Humidity sensors based on polymer thin films. *Sens. Actuators, B* 1996, 35, 85-90.

2. Lewis, J. S.; Weaver, M. S. Thin-film permeation-barrier technology for flexible organic light-emitting devices. *IEEE J. Sel. Top. Quantum Electron.* 2004, 10, 45-57.

3. Alcoutlabi, M.; McKenna, G. B. Effects of confinement on material behaviour at the nanometre size scale. *J. Phys.: Condens. Matter* 2005, 17, R461-R524.

4. Baschnagel, J.; Binder, K. On the Influence of hard walls on structural-properties in polymer glass simulation. *Macromolecules* 1995, 28, 6808-6818.

5. Binder, K.; Horbach, J.; Vink, R.; De Virgiliis, A. Confinement effects on phase behavior of soft matter systems. *Soft Matter* 2008, 4, 1555-1568.

6. Binder, K.; Puri, S.; Das, S. K.; Horbach, J. Phase separation in confined geometries. *J. Stat. Phys.* 2010, 138, 51-84.

7. de Gennes, P. G. Glass transitions in thin polymer films. *Eur. Phys. J. E* 2000, 2, 201-205.

8. Ellison, C. J.; Kim, S. D.; Hall, D. B.; Torkelson, J. M. Confinement and processing effects on glass transition temperature and physical aging in ultrathin polymer films: novel fluorescence measurements. *Eur. Phys. J. E: Soft Matter Biol. Phys.* 2002, 8, 155-66.

9. Keddie, J. L.; Jones, R. A. L.; Cory, R. A. Size-dependent depression of the glass-transition temperature in polymer-films. *Europhys. Lett.* 1994, 27, 59-64.

10. Priestley, R. D. Physical aging of confined glasses. *Soft Matter* 2009, 5, 919-926.

11. Priestley, R. D.; Broadbelt, L. J.; Torkelson, J. M. Physical aging of ultrathin polymer films above and below the bulk glass transition temperature: Effects of attractive vs neutral polymer-substrate interactions measured by fluorescence. *Macromolecules* 2005, 38, 654-657.

12. Briscoe, B. J.; Fiori, L.; Pelillo, E. Nano-indentation of polymeric surfaces. *J. Phys. D Appl. Phys.* 1998, 31, 2395-2405.

13. Dimitriadis, E. K.; Horkay, F.; Maresca, J.; Kachar, B.; Chadwick, R. S. Determination of elastic moduli of thin layers of soft material using the atomic force microscope. *Biophys. J.* 2002, 82, 2798-2810.

14. Sun, Y. J.; Akhremitchev, B.; Walker, G. C. Using the adhesive interaction between atomic force microscopy tips and polymer surfaces to measure the elastic modulus of compliant samples. *Langmuir* 2004, 20, 5837-5845.

15. Tranchida, D.; Piccarolo, S.; Loos, J.; Alexeev, A. Mechanical characterization of polymers on a nanometer scale through nanoindentation. A study on pile-up and viscoelasticity. *Macromolecules* 2007, 40, 1259-1267.

16. Dokukin, M. E.; Sokolov, I. On the measurements of rigidity modulus of soft materials in nanoindentation experiments at small depth. *Macromolecules* 2012, 45, 4277-4288.

17. Cappella, B.; Kaliappan, S. K.; Sturm, H. Using AFM force-distance curves to study the glass-to-rubber transition of amorphous polymers and their elastic-plastic properties as a function of temperature. *Macromolecules* 2005, 38, 1874-1881.

18. Tranchida, D.; Piccarolo, S.; Soliman, M. Nanoscale mechanical characterization of polymers by AFM nanoindentations: Critical approach to the elastic characterization. *Macromolecules* 2006, 39, 4547-4556.

19. Butt, H. J.; Cappella, B.; Kappl, M. Force measurements with the atomic force microscope: Technique, interpretation and applications. *Surf. Sci. Rep.* 2005, 59, 1-152.

20. Passeri, D.; Rossi, M.; Tamburri, E.; Terranova, M. L. Mechanical characterization of polymeric thin films by atomic force microscopy based techniques. *Anal. Bioanal. Chem.* 2013, 405, 1463-1478.

21. Domke, J.; Radmacher, M. Measuring the elastic properties of thin polymer films with the atomic force microscope. *Langmuir* 1998, 14, 3320-3325.

22. Geng, K. B.; Yang, F. Q.; Druffel, T.; Grulke, E. A. Nanoindentation behavior of ultrathin polymeric films. *Polymer* 2005, 46, 11768-11772.

23. Miyake, K.; Satomi, N.; Sasaki, S. Elastic modulus of polystyrene film from near surface to bulk measured by nanoindentation using atomic force microscopy. *Appl. Phys. Lett.* 2006, 89, 031925.

24. Zhou, J.; Komvopoulos, K. Surface and interface viscoelastic behaviors of thin polymer films investigated by nanoindentation. *J. Appl. Phys.* 2006, 100, 11.

25. Tweedie, C. A.; Constantinides, G.; Lehman, K. E.; Brill, D. J.; Blackman, G. S.; Van Vliet, K. J. Enhanced stiffness of amorphous polymer surfaces under confinement of localized contact loads. *Adv. Mater.* 2007, 19, 2540-2546.

26. Xu, W.; Chahine, N.; Sulchek, T. Extreme hardening of PDMS thin films due to high compressive strain and confined thickness. *Langmuir* 2011, 27, 8470-8477.

27. Watcharotone, S.; Wood, C. D.; Friedrich, R.; Chen, X. Q.; Qiao, R.; Putz, K.; Brinson, L. C. Interfacial and substrate effects on local elastic properties of polymers using coupled experiments and modeling of nanoindentation. *Adv. Eng. Mater.* 2011, 13, 400-404.

28. Silbernagl, D.; Cappella, B. Mechanical properties of thin polymer films on stiff substrates. *Scanning* 2010, 32, 282-293.

29. Perriot, A.; Barthel, E. Elastic contact to a coated half-space: Effective elastic modulus and real penetration. *J. Mater. Res.* 2004, 19, 600-608.

30. Clifford, C. A.; Seah, M. P. Modelling of nanomechanical nanoindentation measurements using an AFM or nanoindenter for compliant layers on stiffer substrates. *Nanotechnology* 2006, 17, 5283-5292.

31. Clifford, C. A.; Seah, M. P. Nanoindentation measurement of Young's modulus for compliant layers on stiffer substrates including the effect of Poisson's ratios. *Nanotechnology* 2009, 20, 145708.

32. Keddie, J. L.; Jones, R. A. L.; Cory, R. A. Interface and surface effects on the glass-transition temperature in thin polymer-films. *Faraday Discuss.* 1994, 98, 219-230.

33. Hutter, J. L.; Bechhoefer, J. Calibration of atomic-force microscope tips. *Rev. Sci. Instrum.* 1993, 64, 1868.

34. Johnson, K. L.; Kendall, K.; Roberts, A. D. Surface energy and contact of elastic solids. *Proc. R. Soc. London, Ser. A* 1971, 324, 301-313.

35. Nielsen, L. E. Mechanical properties of polymers; Van Nostrand Reinhold: New York, 1962.

36. Shah, Q. H. Impact resistance of a rectangular polycarbonate armor plate subjected to single and multiple impacts. *Int. J. Impact Eng.* 2009, 36, 1128-1135.

37. Brandrup, J.; Immergut, E. H. Polymer handbook; 3rd ed.; Wiley: New York, 1989.

38. Teichroeb, J. H.; Forrest, J. A. Direct imaging of nanoparticle embedding to probe viscoelasticity of polymer surfaces. *Phys. Rev. Lett.* 2003, 91, 016104.

39. Karim, T. B.; McKenna, G. B. Evidence of surface softening in polymers and their nanocomposites as determined by spontaneous particle embedment. *Polymer* 2011, 52, 6134-6145.

40. Forrest, J. A.; DalnokiVeress, K.; Dutcher, J. R. Interface and chain confinement effects on the glass transition temperature of thin polymer films. *Phys. Rev. E* 1997, 56, 5705-5716.

41. Zoller, P.; Walsh, D. J. Standard pressure-volume-temperature data for polymers; Technomic Publshing Co.: Lancaster, PA, 1995.

42. Soles, C. L.; Douglas, J. F.; Wu, W. L.; Dimeo, R. M. Incoherent neutron scattering as a probe of the dynamics in molecularly thin polymer films. *Macromolecules* 2003, 36, 373-379.

43. Wu, S. H. Chain structure, phase morphology, and toughness relationships in polymers and blends. *Polym. Eng. Sci.* 1990, 30, 753-761.

44. Ferguson, R. J.; Marshall, G. P.; Williams, J. G. Fracture of rubber-modified polystyrene. *Polymer* 1973, 14, 451-459.

45. Inoue, R.; Kanaya, T.; Nishida, K.; Tsukushi, I.; Shibata, K. Inelastic neutron scattering study of low energy excitations in polymer thin films. *Phys. Rev. Lett.* 2005, 95, 056102.

46. Kanaya, T.; Tsukushi, I.; Kaji, K.; Gabrys, B. J.; Bennington, S. A.; Furuya, H. Localized picosecond-scale process in glassy poly-(methyl methacrylate) far below T_g. *Phys. Rev. B* 2001, 64, 144202.

47. Soles, C. L.; Douglas, J. F.; Wu, W. L.; Dimeo, R. M. Incoherent neutron scattering and the dynamics of confined polycarbonate films. *Phys. Rev. Lett.* 2002, 88, 037401.

48. Dequidt, A.; Long, D. R.; Sotta, P.; Sanseau, O. Mechanical properties of thin confined polymer films close to the glass transition in the linear regime of deformation: Theory and simulations. *Eur. Phys. J. E* 2012, 35, 61.

49. Long, D.; Lequeux, F. Heterogeneous dynamics at the glass transition in van der Waals liquids, in the bulk and in thin films. *Eur. Phys. J. E* 2001, 4, 371-387.

50. Merabia, S.; Sotta, P.; Long, D. Heterogeneous nature of the dynamics and glass transition in thin polymer films. *Eur. Phys. J. E* 2004, 15, 189-210.

51. Riggleman, R. A.; Douglas, J. F.; de Pablo, J. J. Antiplasticization and the elastic properties of glass-forming polymer liquids. *Soft Matter* 2010, 6, 292-304.

Chapter 3

The Elastic Mechanical Response of Nanoscale Thin Films of Miscible Polymer/Polymer Blends

3.1 Introduction

The mechanical properties of thin polymer films are of critical importance in diverse applications, from coatings and nano-imprint lithography to functional applications that include organic electronics and energy conversion. Molecular dynamics (MD) simulations [1,2], finite element analysis (FEA) [3,4], thin film buckling experiments [5,6], Brillouin light scattering (BLS) [7,8], and nanoindentation measurements [9-17] have provided valuable insights into the mechanical behavior of polymer films in the nanoscale thickness range (from tens of nanometers to hundreds of nanometers). BLS experiments indicate that the high-frequency elastic properties of supported polystyrene (PS) and poly(methyl methacrylate) (PMMA) films are independent of film thickness, for films as thin as $h \sim 40$ nm [7,8]. Thin film buckling studies of the elastic moduli of PS

and of a range of methacrylate based polymeric thin films, each supported on soft poly(dimethylsiloxane) substrates, reveal that the apparent moduli deviate from the bulk, decreasing with decreasing film thickness, for thicknesses less than approximately 40-80 nm [5,6]. MD simulations corroborate these observations, indicating that when the polymer film is sufficiently thin the elastic modulus, or stiffness, decreases with decreasing film thickness [1,2]. This behavior is associated with the fact that the monomer segments at the free surface of a linear-chain polymer system possess enhanced configurational freedom (enhanced mobility) in comparison to the bulk. Therefore, when h is sufficiently small, the average modulus of the film becomes smaller than the bulk. The exact thickness h at which the deviation occurs depends on the difference between the temperature of the measurement T and the glass transition temperature T_g of the polymer ($T < T_g$).

In this paper we are interested in the elastic mechanical moduli of polymer films with thicknesses on the order of hundreds of nanometers. Specifically of interest here is the general finding by nanoindentation measurements of polymer films supported by stiff substrates that films below a threshold thickness h_t exhibit elastic moduli that are enhanced in relation to the bulk (substrate effect); the threshold thicknesses are a few hundred nanometers [9-17]. Nanoindentation, in contrast to BLS and the buckling experiments, involves the impact of a probe with the surface of a sample; this has the effect of imposing a stress field that propagates into the sample at distances hundreds of nanometers. Contact mechanics principles are used to extract the mechanical properties [9-17]. Numerical studies [3,4,18], combined with experimental studies [16,17], suggest that the enhancement of the effective moduli of a thin film is associated with the

propagation of the indentation-induced stress field throughout the entire film, hundreds of nanometers, and the interaction of the field with the underlying substrate [16,17]. FEA studies further suggest that the enhanced moduli in these films may be rationalized entirely in terms of the moduli of the polymer and the stiff substrate and the Poisson's ratio of the film [3,4].

Recently we showed, using an atomic force microscopy (AFM) nanoindentation technique, that the elastic mechanical responses of PS and PMMA films, hundreds of nanometers thick, supported by silicon oxide (SiO_x) substrates are virtually identical [17]. They exhibited similar threshold thicknesses, $h_t \sim 450$ nm. It is noteworthy that PS exhibits nonwetting interactions with SiO_x interface [19], in contrast to the PMMA, whose interactions with SiO_x are strong [20]. We also showed that the moduli and the threshold thicknesses responses of polycarbonate (PC), and of poly(vinyl chloride) (PVC) films, each supported by SiO_x substrates, were significantly lower than those of PS and PMMA: h_t(PC) $\sim$ 300 nm and h_t(PVC) $<$ 200 nm. The mechanical responses of these polymers could not be rationalized in terms of the elastic moduli, the Poisson's ratios of the polymers, or with the polymer/substrate interfacial interactions. We showed that the relative values of h_t, instead, correlated well with the vibrational force constants κ of the individual polymers.

It would appear that deviations of the elastic modulus of thin films from the bulk would be attributed to two different reasons. For the thinnest films, the deviation is associated with differences between the configurational freedoms of chain segments, and interactions, at the external interfaces and those from the bulk. In the second, the deviation is associated with the propagation of an external indentation imposed stress

field through the film. The extent of the propagation, as mentioned above, is dependent on the polymer; it is significant in PS compared to PVC and PC. Hence an important question would be to what extent could the mechanical response of a polymer be "tailored" or suppressed? New insights into the mechanical response of thin polymer films may be gained by investigating the response of miscible polymer/polymer thin film blends of varying thicknesses, tens to hundreds of nanometers. Miscible blends are interesting because they are known to exhibit properties (T_gs, specific volume, bulk mechanical properties, permeability, etc.) that are typically different, often enhanced, from the average behavior of the blend [21]. With a miscible blend, preferential interactions between the blend components and the external interfaces lead to interfacial compositions that differ from the bulk. Therefore, a miscible blend for which different experimental parameters, including bulk composition, interfacial compositions, T_gs, specific volumes, would be appropriate.

A good candidate would be PS and tetramethyl bisphenol-A polycarbonate (TMPC); much is known about this blend [22-30]: (1) the bulk PS/TMPC blends exhibit lower critical solution temperature above ~240 ℃ [25-27]; (2) compositional dependence of T_g show large negative deviations from linear additivity [25-27]; (3) the specific volume exhibit negative deviations from rule of mixture [23,29]; (4) the T_g of PS film (~100 ℃) is much lower than that of TMPC film (~220 ℃) [30]. Additionally, for PS/TMPC thin film blends supported on SiO_x substrates, the free surface is enriched with PS due to its lower surface energy compared to TMPC [30-32]. TMPC has highly specific interactions (hydrogen bonding) with SiO_x substrate, so it preferentially enriches the substrate, typically forming a thin layer [30-31].

Our central findings for PS/TMPC blends in the thickness range 200 nm < h < 700 nm include the fact that the effective reduced moduli of PS (K_{PS}) is larger than the effective reduced moduli of TMPC (K_{TMPC}) and moreover $h_{t,PS} \sim 1.5\ h_{t,TMPC}$. Additionally, the effective modulus of each blend $K_{PS/TMPC} \approx (1 - \phi)K_{PS} + \phi K_{TMPC}$, where ϕ is the weight fraction of TMPC. The effects of the differences in the T_gs of the components, the specific volumes, and the changes in interfacial interactions/compositions appear not to be significant on the mechanical response of the PS/TMPC blend films. The elastic mechanical response of this system could not be reconciled in terms of the macroscopic elastic moduli, Poisson's ratios, and interfacial interactions between the polymer and the external interfaces. Instead, the behavior is strongly correlated with the local vibrational constants [33,34], κ, of the materials (individual components and blends), measured using incoherent neutron scattering.

3.2 **Experimental Section**

Solutions of PS (Pressure Chemical, M_w = 49 kg/mol, M_w/M_n = 1.06) and TMPC (Bayer, M_w = 37.9 kg/mol, M_w/M_n = 2.75) were prepared separately using toluene as the solvent; they were mixed with different weight ratios (0:1, 0.25:0.75, 0.5:0.5, 0.75:0.25, and 1:0). Thin films of PS/TMPC blends were prepared by spin-coating solutions onto oxidized (~1.8 nm native oxide layer) silicon substrates (Wafer World). Each film was annealed in a vacuum oven at 10 ℃ above the T_g of the thin film blends for 4 h in order to remove residual solvent. Film thicknesses were measured using spectroscopic ellipsometer (JA Woolam, M-2000).

The nanoindentation measurements were performed using an AFM (Asylum Research, MFP-3D), under conditions of constant temperature, T = 30 ℃. A hemispherical AFM tip (radius $R \sim 540$ nm) was prepared by annealing an AFM probe (NanoWorld, NCH) in air for approximately 4 h at 1200 ℃. The shape of the tip was examined prior to and after the measurement using a scanning electron microscope (FEI, Nova Nanolab 200). The sensitivity of the AFM cantilever was calibrated on a mica substrate, and the spring constant of the cantilever, measured by thermal tune method [35], was approximately 42 N/m. The surface root-mean-square (RMF) roughness of the films, measured over the surface area of 5 × 5 μm^2, was 0.32 nm on average. During all nanoindentation measurements, the maximum force, F_{max}, was kept at a constant value of 400 nN. The indentation rate of 40 nm/s was maintained constant under a closed loop mode.

Force−distance (FD) curves obtained from the nanoindentation measurements were fit using the Johnson-Kendall-Roberts (JKR) model which indicates that the radius of contact a between the indenter and sample surface is [36]

$$a^3 = \frac{R}{K}\left[F + 3\pi RW + \left(6\pi RWF + (3\pi RW)^2\right)^{1/2}\right] \qquad (3.1)$$

The indentation depth, d, is

$$d = \frac{a^2}{R} - \left(\frac{8\pi Wa}{3K}\right)^{1/2} \qquad (3.2)$$

In these equations R is the radius of the indenter, K is the effective reduced modulus, F is the applied force, and W is the work of adhesion. According to the JKR model, separation between the indenter and sample surface will occur when the "pull-off" force (or

maximum adhesion force) is greater than $F_{ad} = -3/2(\pi RW)$ [36], and W was estimated from the corresponding pull-off force in each FD curve. The reduced modulus, K, is defined in terms of the elastic modulus of the polymer, $E_{polymer}$, and of the AFM tip, E_{tip}, and Poisson's ratio of the polymer, $\nu_{polymer}$, and of the tip, ν_{tip}: $1/K = (3/4)((1 - \nu_{polymer}^2)/E_{polymer} + (1 - \nu_{tip}^2)/E_{tip})$; since $E_{tip} \gg E_{polymer}$, $1/E_r \approx (3/4)((1 - \nu_{polymer}^2)/E_{polymer})$ [37]. Since the Poisson's ratio of the PS/TMPC blends and TMPC is unknown, the mechanical response will be analyzed in terms of K, which does not require knowledge of the material's Poisson's ratio. The JKR analysis is shown to be appropriate for analyzing the mechanical response of polymer films indented with a large radius tip [38,39].

We also used the Derjaguin-Muller-Toporov (DMT) model [40], which is generally appropriate for indentation measurements using a small and sharp tips [38,41], to fit same FD curves. The estimated values of K are consistently lower than those estimated using the JKR model; these data are reported in Figure A.1. Despite the slight differences in the values of K estimated with the JKR and DMT models, the trends of overall elastic mechanical responses are virtually identical.

3.3 **Results and Discussion**

A typical FD curve, which denotes the force between the AFM tip and the surface of the film as a function of the relative position of the tip normal to the film surface, is shown in Figure 3.1a. In this figure the curve representing the approach (represented by open squares) and that representing the retraction (represented by open circles) overlap, which is indicative of the absence of hysteresis in the contact regime. This indicates that the measurements were performed in the elastic deformation regime [38]. Mechanical

properties were extracted from FD curves by fitting K and the distance, d (see Figure 3.1a), in the contact regime of the retraction curves using the JKR model [39]. The fit is represented by solid line in Figure 3.1a, and was obtained using the least-squares method. The JKR method has been shown to be a more accurate model for analyzing polymer films than the Hertz model for shallow indentations where adhesion between the indenter and the surface of sample is not negligible [39].

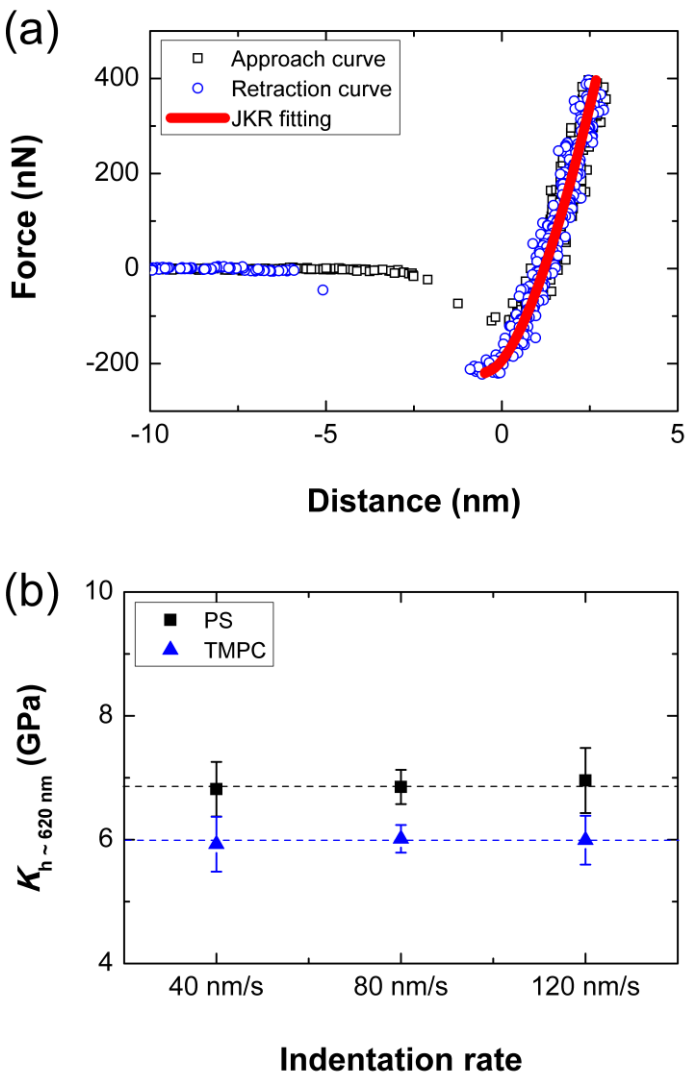

Figure 3.1 (a) A typical FD curve obtained from a nanoindentation measurement of a film of $h \sim 620$ nm thick TMPC film is shown. (b) The K is shown for PS and TMPC films. Each data point is an average of 11 nanoindentation experiments, and the dashed lines are guides for the eyes.

Nanoindentation measurements were performed at different indentation rates (from 40 to 120 nm/s) on PS and TMPC films of $h \sim 620$ nm. The values of K were independent of the indentation rates, as shown in Figure 3.1b. The absence of a hysteresis effect in the FD curves, and the indentation rate independent K, indicates that viscoelastic effects are negligible in our measurements. This is not unexpected, considering that the

T_gs of the thin film blends are well above the temperature at which our measurements were performed (T = 30 ℃).

AFM nanoindentation measurements were also performed on a series of PS/TMPC thin film blends of similar thicknesses h ~620 nm. The moduli K extracted from the data are plotted as a function of TMPC weight fraction ϕ in Figure 3.2. Note that F_{max} was kept at a constant value of 400 nN during the nanoindentation measurements. The K of the TMPC film is lower than that of the PS film. The K of PS/TMPC blend films decrease linearly with increasing TMPC weight fraction: $K_{PS/TMPC} = (1 - \phi)K_{PS} + \phi K_{TMPC}$. The magnitudes of the moduli are independent of change in the glass transition temperatures of the blends, which vary by over 100° ($T_{g,PS}$ = 100 ℃, $T_{g,TMPC}$ = 220 ℃) [30]. The T_g of the thin film blends increased monotonically, in a nonlinear manner, with increasing TMPC weight fraction [30]. However, K decreases linearly with increasing TMPC weight fraction, as shown in Figure 3.2.

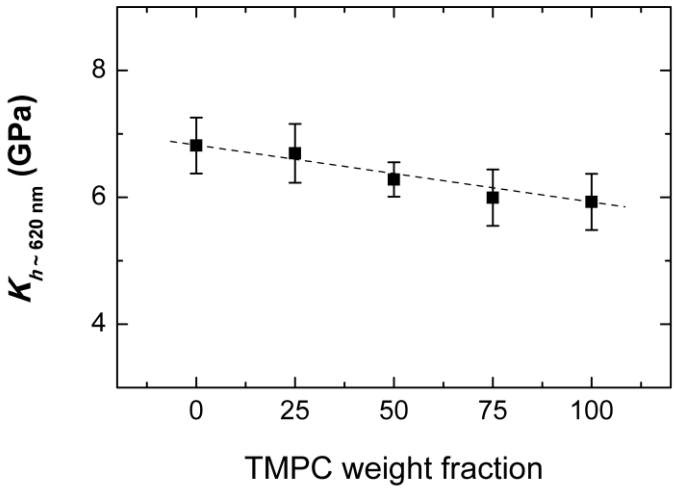

Figure 3.2 K of the PS/TMPC blend films of thickness, $h \sim 620$ nm, at fixed maximum force, $F_{max} = 400$ nN, are plotted as a function of the weight fraction of TMPC, ϕ. Each data point is an average of 15 nanoindentation measurements, and the dashed line is guide for the eyes.

Our results indicate that the magnitudes of K were insensitive to the PS surface enrichment; PS has a lower surface energy [30-32]. Considering the small indentation depths $d < 3$ nm of our measurements, one might anticipate a positive deviation of K from linear additivity, due to the enrichment of free surface layer by PS, which possesses the larger modulus K. However, the fact that the compositional dependence of $K_{PS/TMPC}$ is described by an effective medium approximation indicates that the surface enrichment does not influence the overall mechanical response of polymer thin films in this thickness range. Considering the length scale of the average contact radius, $a_{ave} \sim 50$ nm, between the AFM tip and the surface of blend films, which provides information about the volume of material being probed, it is not surprising that the nanoindentation measurements are insensitive to the surface enrichment.

The free surface structure, as suggested earlier, has been shown to influence the elastic response of polymer films. The reduction of the modulus of films with thicknesses less than 100 nm is associated with the fact that near a free surface the configurational freedom of chain segments is enhanced (decrease monomer density) in comparison to the bulk; hence, the free surface has a lower modulus. This lower surface modulus becomes important when the film is sufficiently thin; it is the reason the average modulus of a sufficiently thin film is lower than the bulk. A striking feature of this phenomenon is that it is temperature dependent, as shown by experiment and simulations. In the glassy state, $T \ll T_g$, the effect is smallest. However, as T approaches T_g from below, the length scale of the region where the enhancement of the configurational freedom (i.e., sometimes referred to as a "liquid-like" layer) increases [42,43]. Therefore, the critical film thickness below which the modulus decreases would increase with increasing temperature. In light of this, the film thickness dependence is more significant as T approaches T_g, from below. Whereas MD simulations clearly predict this effect, FEA, lacking microscopic details, necessarily fails to capture this behavior [1,2].

With regard to films in the nanoscale thickness regime, as mentioned earlier, the indentation-induced stress field is understood to extend over a large region [3,4,44]. In our previous study, we showed that the stress field propagates several hundreds of nanometers into PS, PMMA, and PC films even for indentation depths $d < 3$ nm [17]. Since the stress field imposed by indentation extends over much larger length scales (on the order of hundreds of nanometers) compared to the length scale of both the free surface layer and self-concentration effects [34] (local PS-rich and TMPC-rich domains on the order of nanometers), PS/TMPC blends can be considered as a homogeneous

medium. It is important to note that the mechanical behavior of thin polymer films, typically in the thickness range of less than 100 nm, have also been well described in terms of dynamic heterogeneity models by Long and co-workers [45]. This model makes specific predictions for the mechanical moduli of films confined between two attractive "walls". Further, this model carefully describes the effects of interfaces on the mechanical properties of very thin films, nanometers or tens of nanometers thick. An explanation for our observations would therefore likely be related to the elastic properties of the polymer and not the interfacial effects.

The reduced moduli $K(h)$ are plotted for PS, a 50/50 wt % blend of PS/TMPC, and TMPC films as a function of film thickness in Figure 3.3a. The $K(h)$ for all the films increase with decreasing h. As mentioned above, the enhanced mechanical moduli of sufficiently thin polymer films have been understood in terms of propagation of the stress field through the film and its interaction with the stiff underlying substrate [16,17]. Interestingly, the threshold thickness of the blend, h_t(PS/TMPC), is lower than that of PS and higher than that of TMPC: h_t(PS) ~ 440 nm, h_t(50/50 blend) ~ 400 nm, and h_t(TMPC) ~ 320 nm. In order to compare the magnitude of substrate effect, the $K(h)$ in Figure 3.3a are normalized with an average K, for $h > h_t$. The values of $K(h)/E_r(h > h_t)$ are plotted as a function of the ratio of contact radius to film thickness a/h in Figure 3.3b. Note that throughout the thickness range, $h > h_t$, the magnitude of the modulus of the 50/50 blend is approximately equal to the average of the moduli of the components.

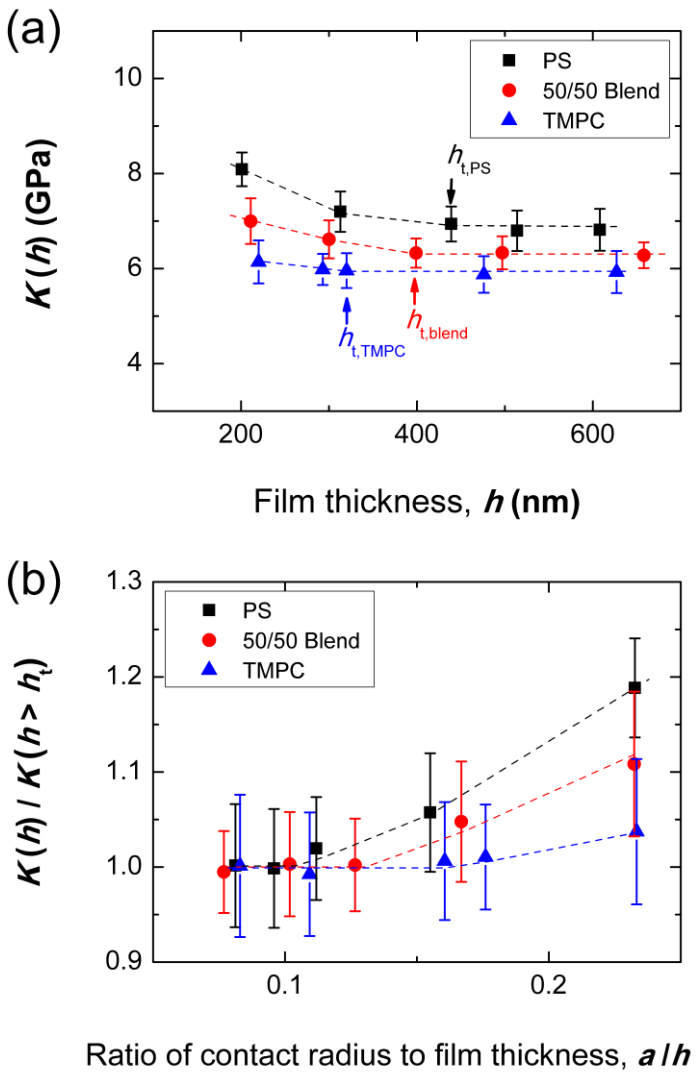

Figure 3.3 (a) Effective reduced moduli, $K(h)$, for PS, a 50/50 wt % blend of PS/TMPC, and TMPC films are plotted as a function of film thickness, h. (b) $K(h)$ normalized with average effective moduli for $h > h_t$, $K(h > h_t)$, and plotted as a function of ratio of contact radius to film thickness, a/h. The maximum force, F_{max}, was kept at a constant value of 400 nN for all the measurements. Each data point is an average of 15 nanoindentation measurements, and dashed lines are guides for the eyes.

Since the stress field propagates throughout a film, provided it is sufficiently thin, then the nature of the interactions between the polymer and the substrate would be important. Weak polymer/substrate interactions could influence the effect of the interfacial stress transfer and hence the modulus. Watcharotone et al. suggested that the

effective modulus of thin polymer films may also be influenced by the polymer/substrate interfacial interactions [16]. They performed nanoindentation measurements on PMMA films supported by oxidized silicon, SiO_x, substrates. Evidence of strong attractive interactions between PMMA segments and SiO_x were reported in this system. Such interactions (hydrogen bonding) are responsible for the enhancement of the T_g of thin PMMA films ($h < \sim 100$ nm) on SiO_x, beyond that of the bulk [20]. The enhancement they showed was beyond that which could be rationalized solely by contact mechanics based FEA simulations. Hence, the interactions of the polymer with the substrate may influence the elastic response, provided the film is sufficiently thin.

However, the effect of interactions between the substrate and the TMPC-rich layer of the blend is not important, as we now show for thicker films. In the PS/TMPC blend, as mentioned above, the substrate is enriched with TMPC, due to highly specific interactions (hydrogen bonding) between TMPC segments and SiO_x interface [30,31]. Such strong interfacial interactions between polymer segments and substrate would enhance the local density profile in the vicinity of polymer/substrate interface on a length scale of few monomers [46,47]. This enhanced local density implies that the local mechanical modulus would increase on a comparable length scale. However, these effects are not apparent in our data. In fact, the magnitude of substrate effect for TMPC films is even smaller than that for PS films. Specifically, the normalized values of $K(h)$ in Figure 3.3b increase at much larger values of a/h for TMPC films compared to PS films.

More recently, Cheng et al. performed AFM nanoindentation on cross sections of PMMA films supported by SiO_x and PMMA films supported by alumina, Al_2O_3, substrates [41]. Note that while PMMA/SiO_x interfacial interactions are highly specific

leading to the enhancements of T_g in thin films [20], the opposite is true for PMMA/Al_2O_3 [48]. However, regardless of the differences between the polymer/substrate interfacial interactions, PMMA/SiO_x and PMMA/Al_2O_3 exhibited similar mechanical responses. They suggested that mechanical properties are more strongly influenced by geometric confinement than by the interfacial interactions between the polymer and the substrates.

Having ruled out the interfacial effects, we now consider the macroscopic elastic properties. Using a numerical method, Perriot and Barthel, more specifically, suggested that there exists a transition from bulk-like to a substrate-like mechanical response as the values of a/h increased [18]. This transition shifts to smaller a/h with a decreasing mismatch between the reduced moduli of the film and the substrate. By means of FEA, Clifford and Seah reported that the normalized reduced moduli, $(E^* - E_L^*)/(E_S^* - E_L^*)$, where E_L^* is the reduced modulus of the film and E_S^* is the reduced modulus of the substrate, when plotted as a function of $(E_L^*/E_S^*)^{0.63}a/h$, are all described by the same curve [3]. Further, it has been shown that the extent of substrate effect increases with increasing Poisson's ratio v of the film, under conditions where E_L^* and E_S^* are fixed [4]. Overall, these numerical studies suggest that the substrate effect may be fully understood in terms of the elastic moduli and Poisson's ratios of the soft film and hard underlying substrate. Note that previously Chung et al. showed that regardless of different input values of the elastic moduli and Poisson's ratios relevant to actual polymers, the FEA fails to account for the elastic mechanical response of supported polymer films [17]. The FEA predictions do not account for the large variations of h_t (i.e., differences in the stress field propagation lengths within a film) for different polymers nor does it account for the

data in Figure 3.3b. This is due to lack of microstructural information on different polymeric materials in the FEA studies [17].

There must exist a more reliable explanation for the elastic mechanical responses of the polymers (Figure 3.3), which we now discuss. Long and co-workers suggest that in the vicinity of T_g, and lower temperatures, the mechanical response of a polymer is characterized by a glassy modulus and a viscous modulus [45,47,49]. This follows from the fact that the dynamics of glass forming liquids is known to be heterogeneous, characterized by domains of length scales $\xi \sim$ nm, where relaxation processes are fast or slow compared to an average relaxations; the domains moreover have a finite lifetime. High-frequency relaxations would be associated with the glassy modulus, and low-frequency fluctuations would be associated with the viscous modulus. Notably Riggleman et al. showed that the structure of a glassy solid is characterized by a local elasticity map [50]. The elasticity varies on length scale of nanometers. These results collectively suggest that the local elasticity of the polymer would be important. Hence, information associated with the local chain stiffness (i.e., vibrational force constants), or a molecular compliance, of polymers should be considered in order to rationalize elastic mechanical response of polymeric materials.

The amplitude of atomic thermal vibration or local chain stiffness of polymers could be measured via incoherent neutron scattering experiments [51,52]. In principle, at low T, the mean-square atomic displacement, $\langle u^2 \rangle$, increases linearly with increasing temperature due to harmonic oscillations, $\langle u^2 \rangle \sim k_b T/\kappa$, where k_b is the Boltzmann constant and κ is the vibrational force constant. At higher T range, due to anharmonic vibrations, the temperature dependence of vibrational motions becomes nonlinear and

increases more rapidly. For PS/TMPC blends, it has been reported that the force constant, κ, is higher for TMPC compared to that of PS and κ of PS/TMPC blend increases with increasing TMPC weight fraction: $\kappa_{TMPC} > \kappa_{50/50\ blend} > \kappa_{PS}$ [33,34]. This is illustrated in Figure 3.4, where a/h and κ exhibit similar dependences on ϕ.

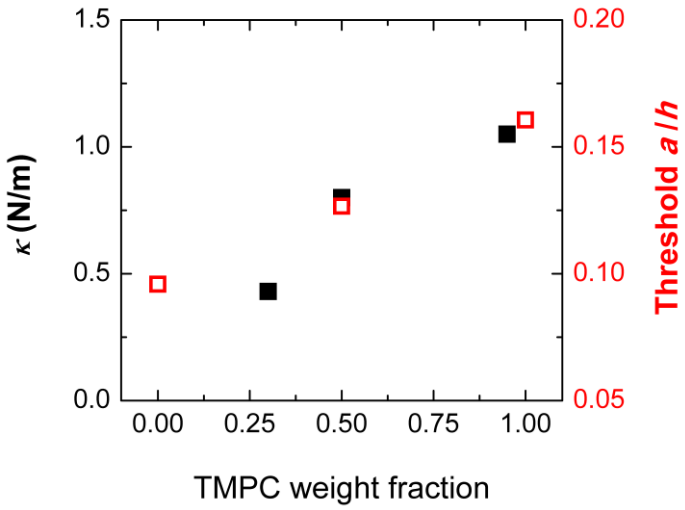

Figure 3.4 Vibrational force constant κ (filled squares, ref 33), and the threshold ratio of contact radius to film thickness a/h (open squares), are plotted as a function of TMPC weight fraction, ϕ. Note that larger values of threshold a/h correspond to lower degree of substrate effect.

We have suggested that the propagation of stress field in polymers would be associated with $\langle u^2 \rangle$ and hence the local chain stiffness, κ [17]. Specifically, for a given a/h value, the magnitude of stress propagation would be larger for a polymer with a smaller value of κ compared to other polymers with larger values of κ, leading to a stronger degree of substrate effect. In agreement, our observations of different degree of substrate effect for PS/TMPC blends could be rationalized in terms of local vibration constant and hence local chain stiffness. Recall that PS films exhibited a larger enhancement in modulus with decreasing film thickness h compared to TMPC films. The

K of the 50/50 blend films was nearly the average of PS and PMMA, in the thickness regime we studied. Under the same degree of elastic deformation, the magnitude of the propagation of the stress field would be larger in PS films than in TMPC films due to the smaller value of κ for PS compared to TMPC. This is manifested in the fact that normalized *K* of PS increases at smaller value of a/h as shown in Figure 3.4 compared to that of TMPC films. For 50/50 blend films, due to the intermediate value of κ, the substrate effect follows the average behavior of PS and TMPC films.

The structure of a miscible blend is heterogeneous, characterized by A-rich and B-rich domains at nanometer length scales, due to self-concentration effects. We speculate that the vibrational force constants of the blend would manifest those of the individual A and B components. This could be the reason that the vibrational fore constant of the mixture is not very different from the weighted average of the vibrational force constants of the blend components. Because the length scale of propagation of the imposed stress field is hundreds of nanometers, which is many orders of magnitude larger than the interfacial excesses of the individual components, it should not be surprising that the interfacial interactions do not influence the modulus measured by the nanoindentation experiments, provided that $h > h_t$.

3.4 **Conclusion**

The elastic mechanical moduli of SiOx supported thin films of PS, TMPC, and their miscible blends, investigated using an AFM nanoindentation, exhibited increases with decreasing film thickness *h*, for $h < h_t$. It is well understood that enhancement of the moduli for $h < h_t$ is due to the propagation and impingement of the indentation induced

stress field with the substrate. The implication of course is that the nanoindentation measurements provide an accurate measure of the actual modulus of a polymer film, supported by a stiff substrate, provided that $h > h_t$. For this reason the nanoindentation experiments are not appropriate for very thin films where the interfacial interactions also influence the mechanical response. The buckling experiments and the BLS would be more appropriate.

The values of h_t are different for each material: h_t(PS) ~ 450 nm and h_t(TMPC) ~ 300 nm. The values of the threshold thicknesses for each blend, h_t(PS/TMPC), were well described by an effective medium approximation. It appears from our results that the differences between the responses of each polymer may be understood in terms of its vibrational force constants κ. For the blend, $\kappa_{PS/TMPC}$ appears to be reasonably described by the weighted average stiffness f PS and f TMPC of the pure components.

Because the induced stress fields propagate hundreds of nanometers, the experimentally measured moduli are indicative of the average compositions of the blends; they would not be sensitive to compositional variations on the order of nanometers. Hence, interfacial effects, which influence the mechanical behavior of much thinner films $h < 100$ nm, as well as effects associated with self-concentrations, which occur on the scale of nanometers, would not be expected to be manifested in such experiments.

3.5 References

1. Bohme, T. R.; de Pablo, J. J. Evidence for size-dependent mechanical properties from simulations of nanoscopic polymeric structures. *The Journal of chemical physics* 2002, *116*, 9939-9951.

2. Yoshimoto, K.; Jain, T. S.; Nealey, P. F.; de Pablo, J. J. Local dynamic mechanical properties in model free-standing polymer thin films. *The Journal of chemical physics* 2005, *122*, 144712.

3. Clifford, C. A.; Seah, M. P. Modelling of nanomechanical nanoindentation measurements using an AFM or nanoindenter for compliant layers on stiffer substrates. *Nanotechnology* 2006, *17*, 5283-5292.

4. Clifford, C. A.; Seah, M. P. Nanoindentation measurement of Young's modulus for compliant layers on stiffer substrates including the effect of Poisson's ratios. *Nanotechnology* 2009, *20*, 145708.

5. Stafford, C. M.; Vogt, B. D.; Harrison, C.; Julthongpiput, D.; Huang, R. Elastic moduli of ultrathin amorphous polymer films. *Macromolecules* 2006, *39*, 5095-5099.

6. Torres, J. M.; Stafford, C. M.; Vogt, B. D. Elastic modulus of amorphous polymer thin films: relationship to the glass transition temperature. *ACS Nano* 2009, *3*, 2677-2685.

7. Sun, L.; Dutcher, J. R.; Giovannini, L.; Nizzoli, F.; Stevens, J. R.; Ord, J. L. Elastic and elasto-optic properties of thin-films of poly(styrene) Spin-Coated onto Si(001). *J. Appl. Phys.* 1994, *75*, 7482-7488.

8. Cheng, W.; Sainidou, R.; Burgardt, P.; Stefanou, N.; Kiyanova, A.; Efremov, M.; Fytas, G.; Nealey, P. F. Elastic properties and glass transition of supported polymer thin films. *Macromolecules* 2007, *40*, 7283-7290.

9. Domke, J.; Radmacher, M. Measuring the elastic properties of thin polymer films with the atomic force microscope. *Langmuir* 1998, *14*, 3320-3325.

10. Geng, K. B.; Yang, F. Q.; Druffel, T.; Grulke, E. A. Nanoindentation behavior of ultrathin polymeric films. *Polymer* 2005, *46*, 11768-11772.

11. Miyake, K.; Satomi, N.; Sasaki, S. Elastic modulus of polystyrene film from near surface to bulk measured by nanoindentation using atomic force microscopy. *Appl. Phys. Lett.* 2006, *89*, 031925.

12. Zhou, J.; Komvopoulos, K. Surface and interface viscoelastic behaviors of thin polymer films investigated by nanoindentation. *J. Appl. Phys.* 2006, *100*, 114329.

13. Tweedie, C. A.; Constantinides, G.; Lehman, K. E.; Brill, D. J.; Blackman, G. S.; Van Vliet, K. J. Enhanced stiffness of amorphous polymer surfaces under confinement of localized contact loads. *Adv. Mater.* 2007, *19*, 2540-2546.

14. Silbernagl, D.; Cappella, B. Mechanical properties of thin polymer films on stiff substrates. *Scanning* 2010, *32*, 282-293.

15. Xu, W.; Chahine, N.; Sulchek, T. Extreme hardening of PDMS thin films due to high compressive strain and confined thickness. *Langmuir* 2011, *27*, 8470-8477.

16. Watcharotone, S.; Wood, C. D.; Friedrich, R.; Chen, X. Q.; Qiao, R.; Putz, K.; Brinson, L. C. Interfacial and substrate effects on local elastic properties of polymers using coupled experiments and modeling of nanoindentation. *Adv. Eng. Mater.* 2011, *13*, 400-404.

17. Chung, P. C.; Glynos, E.; Green, P. F. The elastic mechanical response of supported thin polymer films. *Langmuir* 2014, *30*, 15200-15205.

18. Perriot, A.; Barthel, E. Elastic contact to a coated half-space: Effective elastic modulus and real penetration. *J. Mater. Res.* 2004, *19*, 600-608.

19. Keddie, J. L.; Jones, R. A. L.; Cory, R. A. Size-dependent depression of the glass-transition temperature in polymer-films. *Europhys. Lett.* 1994, *27*, 59-64.

20. Keddie, J. L.; Jones, R. A. L.; Cory, R. A. Interface and surface effects on the glass-transition temperature in thin polymer-films. *Faraday Discuss* 1994, *98*, 219-230.

21. Utracki, L. A.; Wilkie, C. A. *Polymer Blends Handbook*; 2nd ed.; Springer: Netherlands2014.

22. Shaw, M. T. Studies of polymer–polymer solubility using a two-dimensional solubility parameter approach. *Journal of Applied Polymer Science* 1974, *18*, 449-472.

23. Yee, A. F.; Maxwell, M. A. Mechanical-properties of polymer mixtures - Effect of compatibility. *J. Macromol. Sci. Phys.* 1980, *B17*, 543-564.

24. Wisniewsky, C.; Marin, G.; Monge, P. Viscoelastic behavior of compatible polymer blends - Polystyrene tetramethylpolycarbonate. *Eur. Polym. J.* 1984, *20*, 691-695.

25. Fernandes, A. C.; Barlow, J. W.; Paul, D. R. Blends containing tetramethyl bisphenol-A polycarbonate: 1. Styrenic polymers. *Polymer* 1986, *27*, 1788-1798.

26. Guo, W.; Higgins, J. S. Miscibility and kinetics of phase separation in polymer blends of tetramethyl-bisphenol-A polycarbonate and polystyrene. *Polymer* 1990, *31*, 699-706.

27. Kim, C. K.; Paul, D. R. Interaction parameters for blends containing polycarbonates: 1. Tetramethyl bisphenol-A polycarbonate polystyrene. *Polymer* 1992, *33*, 1630-1639.

28. Schneider, H. A.; Dimarzio, E. A. The glass temperature of polymer blends: comparison of both the free-volume and the entropy predictions with data. *Polymer* 1992, *33*, 3453-3461.

29. Liu, J.; Jean, Y. C.; Yang, H. J. Free-volume hole properties of polymer blends probed by positron-annihilation spectroscopy - Miscibility. *Macromolecules* 1995, *28*, 5774-5779.

30. Pham, J. Q.; Green, P. F. The glass transition of thin film polymer/polymer blends: Interfacial interactions and confinement. *J. Chem. Phys.* 2002, *116*, 5801-5806.

31. Kim, E.; Krausch, G.; Kramer, E. J.; Osby, J. O. Surface-directed spinodal decomposition in the blend of polystyrene and tetramethyl-bisphenol-A polycarbonate. *Macromolecules* 1994, *27*, 5927-5929.

32. Pham, J. Q.; Green, P. F. Effective T_g of confined polymer-polymer mixtures. Influence of molecular size. *Macromolecules* 2003, *36*, 1665-1669.

33. Besancon, B. M. Interfacial instabilities and the glass transition in polymer thin films. Ph.D. Thesis, The University of Texas at Austin, 2006

34. Besancon, B. M.; Soles, C. L.; Green, P. F. Glass transition of miscible binary polymer-polymer thin films. *Phys. Rev. Lett.* 2006, *97*, 057801.

35. Hutter, J. L.; Bechhoefer, J. Calibration of atomic-force microscope tips. *Rev. Sci. Instrum.* 1993, *64*, 1868-1873.

36. Johnson, K. L.; Kendall, K.; Roberts, A. D. Surface energy and contact of elastic solids. *Proc. R. Soc. Lon. Ser-A* 1971, *324*, 301-313.

37. Passeri, D.; Rossi, M.; Tamburri, E.; Terranova, M. L. Mechanical characterization of polymeric thin films by atomic force microscopy based techniques. *Anal. Bioanal. Chem.* 2013, *405*, 1463-1478.

38. Butt, H. J.; Cappella, B.; Kappl, M. Force measurements with the atomic force microscope: Technique, interpretation and applications. *Surf. Sci. Rep.* 2005, *59*, 1-152.

39. Dokukin, M. E.; Sokolov, I. On the measurements of rigidity modulus of soft materials in nanoindentation experiments at small depth. *Macromolecules* 2012, *45*, 4277-4288.

40. Derjaguin, B. V.; Muller, V. M.; Toporov, Y. P. Effect of contact deformations on adhesion of particles. *J. Colloid Interf. Sci.* 1975, *53*, 314-326.

41. Cheng, X.; Putz, K. W.; Wood, C. D.; Brinson, L. C. Characterization of local elastic modulus in confined polymer films via AFM indentation. *Macromolecular Rapid Communications* 2015, *36*, 391-397.

42. Tranchida, D.; Piccarolo, S.; Loos, J.; Alexeev, A. Mechanical characterization of polymers on a nanometer scale through nanoindentation. A study on pile-up and viscoelasticity. *Macromolecules* 2007, *40*, 1259-1267.

43. Frieberg, B.; Glynos, E.; Green, P. F. Structural relaxations of thin polymer films. *Phys. Rev. Lett.* 2012, *108*, 268304.

44. Ediger, M. D.; Forrest, J. A. Dynamics near free surfaces and the glass transition in thin polymer films: A view to the future. *Macromolecules* 2014, *47*, 471-478.

45. Dequidt, A.; Long, D. R.; Sotta, P.; Sanseau, O. Mechanical properties of thin confined polymer films close to the glass transition in the linear regime of deformation: theory and simulations. *Eur. Phys. J. E* 2012, *35*, 61.

46. Alcoutlabi, M.; McKenna, G. B. Effects of confinement on material behaviour at the nanometre size scale. *J. Phys. Condens Mat.* 2005, *17*, R461-R524.

47. Long, D.; Lequeux, F. Heterogeneous dynamics at the glass transition in van der Waals liquids, in the bulk and in thin films. *Eur. Phys. J. E* 2001, *4*, 371-387.

48. Ash, B. J.; Schadler, L. S.; Siegel, R. W. Glass transition behavior of alumina/polymethylmethacrylate nanocomposites. *Mater. Lett.* 2002, *55*, 83-87.

49. Merabia, S.; Sotta, P.; Long, D. Heterogeneous nature of the dynamics and glass transition in thin polymer films. *Eur. Phys. J. E* 2004, *15*, 189-210.

50. Riggleman, R. A.; Douglas, J. F.; de Pablo, J. J. Antiplasticization and the elastic properties of glass-forming polymer liquids. *Soft Matter* 2010, *6*, 292-304.

51. Soles, C. L.; Douglas, J. F.; Wu, W. L.; Dimeo, R. M. Incoherent neutron scattering as a probe of the dynamics in molecularly thin polymer films. *Macromolecules* 2003, *36*, 373-379.

52. Inoue, R.; Kanaya, T.; Nishida, K.; Tsukushi, I.; Shibata, K. Inelastic neutron scattering study of low energy excitations in polymer thin films. *Phys. Rev. Lett.* 2005, *95*, 056102.

Chapter 4

Macromolecular Architecture Influences the Elastic Mechanical Response of Thin Supported Polymer Films

4.1 Introduction

Star-shaped macromolecules have been shown to exhibit different physical properties from their linear-chain analogs. Notable examples include differences in the glass transition temperatures [1,2], surface wetting properties [3,4], and physical aging [5,6]. Much of this behavior stems from entropic "packing" effects, inherently associated with their molecular architecture, leading to subtle, yet consequential, changes in structure. Parenthetically, for a star-shaped macromolecule, segments of arms close to the core of the molecule are stretched (crowding effect), and the monomer density profile decreases from the vicinity of the core of the molecule to the chain ends [7-10]. Segments near the core suffer an enhanced loss of conformational entropy, compared to segments near the ends of the arms. The monomer density profile, moreover, increases with increasing number of arms f and/or decreasing molecular weight per arm M_n^{arm}. This effect leads to

enhanced long-range entropic repulsion between neighboring macromolecules [9,11]. For star-shaped molecules with sufficiently high f and low M_n^{arm}, experiments and simulations showed that they exhibit high degree of order due to enhanced intermolecular repulsion [12-14]. With regard to their interfacial behavior, star-shaped macromolecules exhibit lower entropic losses compared to their linear chain analogs of the same degree of polymerization, when adsorbed at interfaces [4,15-18]. The strength of the adsorption, increases with increasing functionalities, f, from $f = 2$. This increase is not monotonic and is suppressed for larger functionalities, due to the enhanced intermolecular repulsion for large f.

Evidence of the influence of structure on the physical properties of star-shaped macromolecules is clear from the f and M_n^{arm} dependence of the surface wetting [3,4] and the thin film glass transition behavior [1,2]. In light of these entropic "packing/deformation" effects on the structure, it would be interesting to investigate the thin film elastic mechanical response of star-shaped macromolecules, of varying functionalities, f, and molecular weights per arm, M_n^{arm}.

An understanding of the mechanical properties of thin polymer films is of critical importance for the performance and reliability of polymeric thin film in different applications. Molecular dynamics (MD) simulations [19,20] and thin film buckling experiments [21,22] have provided important insights into the mechanical properties of linear-chain polymer films in the thickness range of a few tens of nanometers. MD simulations indicate that the elastic modulus or mechanical stiffness of polymer films is lower than that of the bulk for films in this thickness range [19,20]. This behavior is associated with enhanced configurational freedom of polymer segments at the free

surface compared to that of the bulk. Consistent with these simulation studies, buckling experiments on polystyrene (PS) thin films, and a series of poly(methacrylate) thin films, supported by poly(dimethylsiloxane) substrates indicate that the elastic moduli of the thin films decrease with decreasing film thickness h, for $h < 40 \sim 80$ nm [21,22]. Independently, theoretical developments by Long and coworkers, based on dynamic heterogeneity models, also provide a rationalization for such observations and have predicted the elastic response for more general situations for linear-chain polymer films confined between two substrates, for varying temperatures, film thicknesses, and polymer/substrate interfacial interactions [23].

Nanoindentation studies have shown that effective moduli E of thin polymer films supported on stiff substrates would increase with decreasing h or with increasing indentation depth d due to the influence of the non-compliant underlying substrate; this is the so-called "substrate effect" [24-29]. This enhancement of E is due to the propagation of the indentation-induced stress field throughout the entire polymer film and interacting with the substrates, when h is sufficiently small and/or when d is sufficiently large [25,27]. While the macroscopic moduli and the polymer/substrate interactions are important, we recently showed that this behavior, propagation of the externally imposed stress field, is largely associated with the local vibrational force constants (i.e. local chain stiffness) of the specific polymer [27,28].

In this paper we are interested in understanding the elastic mechanical response of thin star-shaped PS (SPS) films supported by silicon oxide (SiO_x) substrates. Atomic force microscopy (AFM) nanoindentation measurements were performed on a series of SPS films, with thicknesses in the range of 200 nm < h < 900 nm, of varying f ($2 < f < 64$)

and M_n^{arm} (9 kg/mol. < M_n^{arm} < 140kg/mol.). Consistent with prior studies we show that E increased with decreasing h, for h less than a threshold thickness, h_t, for all the SPS films we studied. Notably, the modulus of SPS films with f = 64 and M_n^{arm} = 9 kg/mol exhibited a considerably stronger degree of enhancement than other SPS films, with lower functionalities, f < 64. For SPS films with f = 64, the degree of enhancement of E(h < h_t) decreased with increasing M_n^{arm} and eventually exhibited a similar degree of enhancement to that of linear-chain PS (LPS) films. We rationalize the difference in the behavior between the 64-arm stars and the other stars (f < 64) in terms of differences between their structures.

4.2 **Experimental Section**

LPS was purchased from Pressure Chemical and 4, 8, and 64 arm SPS were synthesized by means of anionic polymerization [30,31]. The polymers used in this study are listed in Table 4-1. Thin polymer films were prepared by spin coating solutions of LPS and SPS using toluene as the solvent onto oxidized (~1.7 nm native oxide layer) silicon substrates (Wafer World). Thin films were subsequently annealed under vacuum at a temperature of ~30 ℃ above the bulk T_g of the polymer for 2 h for LPS and for at least 24 h for SPS in order to remove residual solvent. Film thicknesses were measured using spectroscopic ellipsometry (JA Woolam, M-2000).

Table 4-1 A list of the polymers used in this study.

Polymer	M_w (Kg/mol)		PDI
Linear PS-6K (LPS-6K)[a]	5.78 kg/mol		1.05
	Number of Arms (f)[b]	M_n^{arm} (kg/mol)[c]	PDI[d]
PS-4arm-7K (SPS-4-7K)	4	7	1.04
PS-8arm-14K (SPS-8-14K)	8	14	1.03
PS-64arm-9K (SPS-64-9K)	64	9	1.02

[a]Purchased from Pressure Chemical. [b]Number of arms, f, determined by the ratio $(M_w)^{star}/(M_n)^{arm}$. [c]From membrane osmometry in toluene at 35 ℃. [d]From SEC in THF at 40 ℃ calibrated with linear PS standards.

Nanoindentation measurements were performed using an AFM (Asylum Research, MFP-3D), with a hemispherical AFM tip. Measurements were performed under closed loop mode to ensure that the indentation rate of 40 nm/s remained constant. The hemispherical AFM tip (radius, R ~ 550 nm) was prepared by annealing an AFM probe (NanoWorld, NCH) in air for ~3.5 h at 1200 ℃ (Figure 4.1). The shape of the tip was imaged prior to and after nanoindentation measurements using a scanning electron microscope (FEI, Nova Nanolab 200). The sensitivity of the AFM cantilever was calibrated on a mica substrate, and the spring constant, measured by thermal tune method [32], was approximately 30 N/m. The average surface root-mean-square (RMS) roughness measured over the area of 5 × 5 μm^2 was 0.31 nm. All the measurements were performed at a constant temperature of T = 30 ℃, which is well below the bulk T_gs of

LPS and SPS used in this study. Note that a fixed maximum force of F_{max} = 400 nN was used for all the nanoindentation measurements.

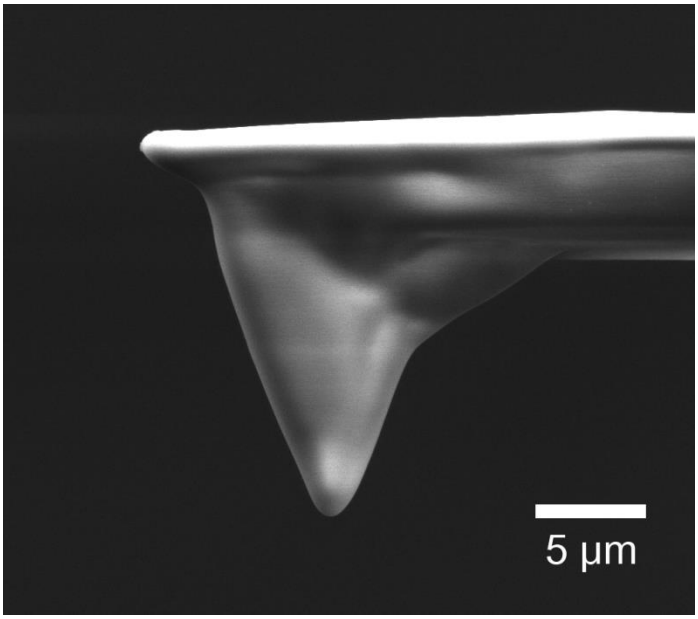

Figure 4.1 A SEM micrograph of the hemispherical AFM tip (radius, R ~ 550 nm) used in this study.

The JKR model was used to analyze FD curves and is described with the following equations [33]:

$$a^3 = \frac{R}{K}[F + 3\pi RW + (6\pi RWF + (3\pi RW)^2)^{1/2}] \quad (4.1)$$

$$d = \frac{a^2}{R} - (\frac{8\pi Wa}{3K})^{1/2} \quad (4.2)$$

In these equations, a is the contact radius, R is the radius of the indenter, K is the reduced modulus, F is the applied force, W is the work of adhesion, and d is the indentation depth. The effective modulus, E, can be estimated from K with the following equation: $1/K = (3/4)\ [(1 - \nu_{polymer}^2)/E_{polymer} + (1 - \nu_{tip}^2)/E_{tip}]$, where $\nu_{polymer}$ is the Poisson's ratio of the

polymer, ν_{tip} is the Poisson's ratio of the AFM tip, $E_{polymer}$ is the elastic modulus of the polymer, and E_{tip} is the elastic modulus of the tip. Since $E_{tip} >> E_{polymer}$, $1/K \approx (3/4)\ [(1 - \nu_{polymer}^2)/E_{polymer}]$ [34]. According to the JKR model, detachment of the indenter from the surface of sample will occur when the pull-off force (or maximum adhesion force) is larger than $F_{ad} = -3/2(\pi\ R\ W)$ [35], and W was estimated from the corresponding FD curve. Poisson' ratio of $\nu = 0.33$ was used for PS [36].

4.3 **Results and Discussion**

A typical force-distance (FD) curve is shown in Figure 4.2, where it is apparent that the approach (represented by open squares) and retraction (represented by open circles) curves overlap, thereby showing no evidence of hysteresis. This indicates that the deformation behavior during nanoindentation measurements was purely elastic [33]. Effective elastic moduli E and indentation depths d were estimated from all FD curves by fitting the retraction curve with the Johnson-Kendall-Roberts (JKR) model (represented by solid line) [37]. Measurements were performed at different indentation rates (from 20 to 80 nm/s) in order to confirm the absence possible viscoelastic effects. E was independent of indentation rates indicating viscoelastic effects are negligible in our nanoindentation measurements. All the nanoindentation measurements were performed in the elastic deformation regime and the maximum force F_{max} was kept at a constant value of $F_{max} = 400$ nN.

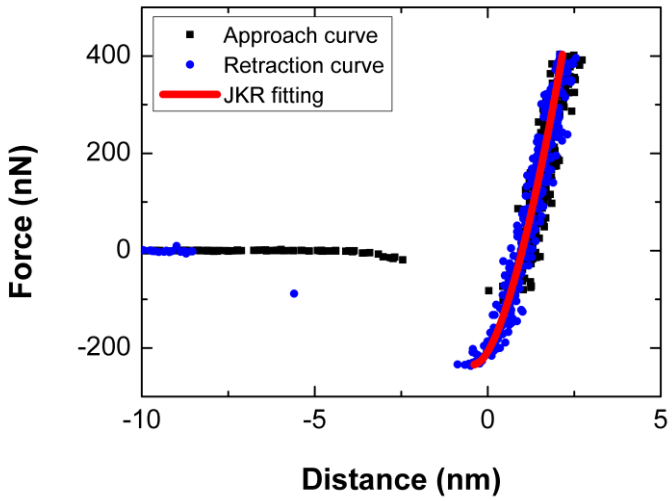

Figure 4.2 Typical FD curve obtain from an AFM nanoindentation measurement of h ~ 870 nm thick 64-arm SPS (M_n^{arm} = 9 kg/mol) film is shown: approach curve (open squares), retraction curve (open circles), and the JKR fitting (solid line).

We investigated the elastic mechanical response of SPS films supported on SiO_x substrates for the following case: the effect of increasing f while M_n^{arm} is fixed at ~10 kg/mol. For this case, the effective moduli $E(h)$ for LPS-6K (M_w = 5.78 kg/mol), SPS-8-14K (f = 8 and M_n^{arm} = 14 kg/mol), and SPS-64-9K (f = 64 and M_n^{arm} = 9 kg/mol) films are plotted as a function of film thickness h in Figure 4.3a. $E(h)$ for all the SPS films increased with decreasing h for $h < h_t$. As mentioned above, the increasing E with decreasing h for sufficiently thin films is understood in terms of substrate effect; indentation-induced stress field propagates throughout the entire polymer film and interacts with the non-compliant substrate, leading to an enhanced local stress field, and hence the magnitude of E [25,27]. The $E(h)$ for SPS-64-9K SPS molecule increases at much higher value of h_t compared to the SPS films with lower functionalities, i.e. f = 8: h_t(SPS-64-9K) ~ 650 nm, while h_t(SPS-8-14K) ~ h_t(LPS-6K) ~ 400 nm. In order to compare the extent of the substrate effect, $E(h)$ values plotted in Figure 4.3a are

normalized with average effective moduli for $h > h_t$, and $E(h)/E(h > h_t)$ are plotted in Figure 4.3b as a function of ratio of contact radius to film thickness, a/h. The a/h dependencies of moduli for SPS-8-14K films are similar to that of their linear-chain analogue, LPS-6K. However, when the functionality is increased to $f = 64$, the moduli increase for lower values of a/h; the degree of enhancement is stronger than other SPS films with lower functionalities.

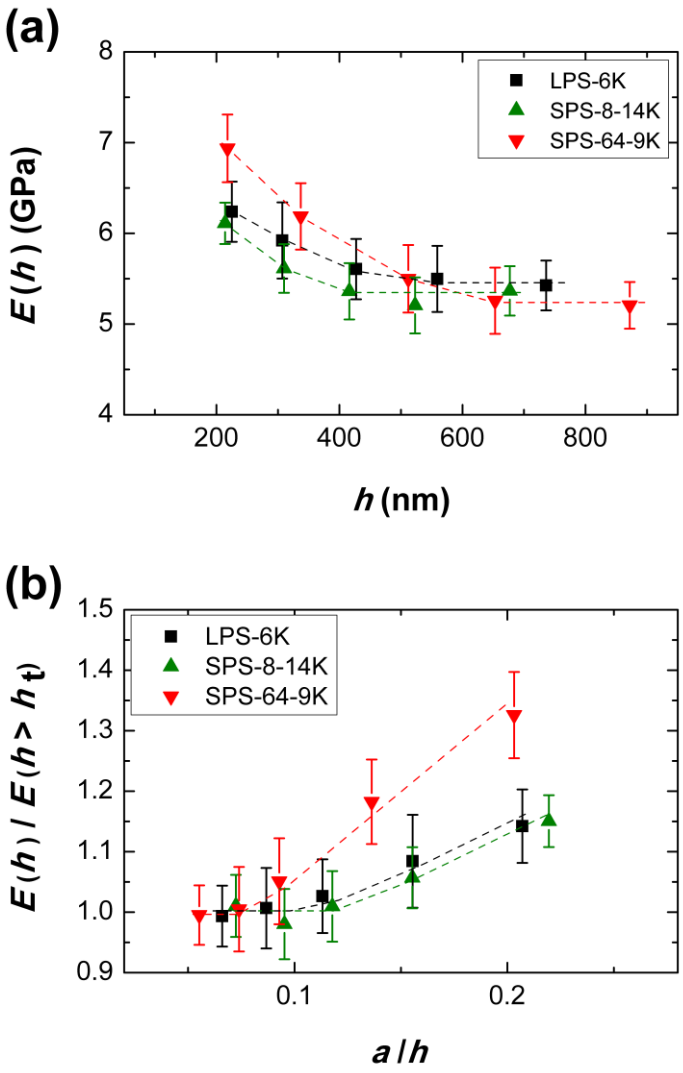

Figure 4.3 (a) Effective moduli, $E(h)$, for LPS (M_w = 6 kg/mol), 8-arm SPS (M_n^{arm} = 14 kg/mol), and 64-arm SPS (M_n^{arm} = 9 kg/mol) films are plotted as a function of film thickness, h. (b) $E(h)$ normalized with average effective moduli for $h > h_t$, E ($h > h_t$) are plotted as a function of ratio of contact radius to film thickness, a/h. Note that maximum force, F_{max}, was fixed at a constant value of 400 nN for all the nanoindentation measurements. Each data point is an average of 15 measurements, and dashed lines are guides for the eyes.

It would be appropriate to comment on the role of interfaces, the free surface and the polymer/substrate interface, on the overall mechanical response of the SPS films. First recall that the average glass transition temperatures of sufficiently thin polymer films are influenced by the strength of interfacial interactions between polymer chains and external interfaces (free surface and substrate). For LPS films supported by SiO_x substrates, it is generally understood that the glass transition temperature at the free surface $T_g^{surface}$ is lower than that of the bulk T_g^{bulk}, i.e. $T_g^{surface} < T_g^{bulk}$. Additionally, the glass transition temperature at the substrate $T_g^{substrate}$ is comparable to T_g^{bulk}, i.e. $T_g^{substrate} \sim T_g^{bulk}$ [38,39]. For this reason, the average T_g of this polymer decreases with decreasing h, for h less than approximately 50 nm. With regard to the SPS films supported by same substrates, it has been shown that $T_g^{surface}$ and $T_g^{substrate}$ are functions of f and M_n^{arm} [1,2]. For sufficiently low f and/or large M_n^{arm}, $T_g^{surface}$ of SPS films exhibit similar behavior compared to those of the LPS films. However, for a functionalities of f = 8 with sufficiently low M_n^{arm}, both $T_g^{surface}$ and $T_g^{substrate}$ were greater than T_g^{bulk} [1]. This behavior is associated with the fact that, based on f and M_n^{arm}, star-shaped molecules suffer lower entropic penalties at interfaces [4,15-18], so packing of the molecules is enhanced at interfaces compared to that of the bulk. However, for the case where f = 64 and $M_n^{arm} \sim 10$ kg/mol, both $T_g^{surface}$ and $T_g^{substrate}$ were comparable to T_g^{bulk}, i.e. $T_g^{surface} \sim T_g^{substrate} \sim T_g^{bulk}$ [2]. In other words, the average T_gs of SPS-64-9K films do not exhibit a dependence on thickness.

Recall the earlier discussion that, for films in the thickness range of less than 40 ~ 80 nm, buckling experiments show that the elastic modulus is a function of thickness [21,22]. This behavior is fundamentally related to interfacial processes, which also

influence the glass transition of thin films. However, having discussed the glass transition temperatures of the SPS molecules, it is apparent that regardless of the interfacial behavior, the a/h dependencies of $E(h)$ for LPS6K and SPS-8-14K shown in Figure 4.3b, are indistinguishable. In other words, there is no connection between the trends in the overall mechanical response and trends in T_g and the interfacial processes. It is noteworthy that these results are not unexpected, considering the following. The length scales over which interfacial interactions at the polymer/substrate or polymer/free surface would affect the modulus is on the order of nanometers [23,40]. By comparison, as shown by finite element analysis and experiments, the actual probing depth of indentation measurements is on the order of few hundreds of nanometers, even for indentation depths of few nanometers [25,27]. For the LPS films supported by SiO_x substrates, we showed that the indentation-induced stress field could extend over ~450 nm thick film even for indentation depths $d < 3$ nm [27,28]. This is also corroborated by the values of $h_t \sim 400$ nm for LPS-6K and SPS-8-14K films shown in Figure 4.3a. Thus, considering the much larger length scale of actual probing depth (on the order of hundreds of nanometers) compared to the thickness of interfacial layers (on the order of few nanometers), we can rule out the effect of interfacial layers on the overall mechanical response of supported SPS films, as determined by nanoindentation measurements.

The rationalization for the very different $E(h)/E(h > h_h)$ vs. a/h response exhibited by the SPS-64-9K films, compared to the other samples, must be based on other reasons. We believe that this response is associated with the structure of the SPS-64-9K macromolecule, which is different from that of the other macromolecules. As mentioned previously, experiments and simulations showed that “star-shaped” macromolecules with

sufficiently large f and small enough M_n^{arm} self-assemble to form highly ordered layers across the film due to strong intermolecular repulsion [12-14]. Moreover, in a recent publication, AFM topographies of SPS-64-9K films revealed layered structures with each layer height corresponding to a length scale of ~ $2R_g$ [2]. Since significant enhancement of $E(h)$ is only observed for 64-arm SPS films with sufficiently low M_n^{arm}, we suggest that the strong degree of enhancement is associated with the structure of SPS-64-9K films.

4.4 Conclusion

In conclusion, the effective moduli $E(h)$ of SPS films supported by SiO_x substrates increase with decreasing film thickness h for $h < h_t$ due to substrate effect. However, the stronger dependence of the moduli on a/h and a larger h_t exhibited by the 64-arm SPS films with sufficiently small M_n^{arm} is associated with its structure, which is composed of highly organized soft colloids. It is suggested the indentation imposed stress may propagate more effectively through the layered structure than its linear chain analogs which are amorphous. The implication of these results is that the overall elastic mechanical response of polymer films supported by stiff substrates can be tailored by tuning their molecular architecture while their chemical structures remain the same.

4.5 References

1. Glynos, E.; Frieberg, B.; Oh, H.; Liu, M.; Gidley, D. W.; Green, P. F. Role of molecular architecture on the vitrification of polymer thin films. *Phys. Rev. Lett.* 2011, 106, 128301.

2. Glynos, E.; Frieberg, B.; Chremos, A.; Sakellariou, G.; Gidley, D. W.; Green, P. F. Vitrification of thin polymer films: From linear chain to soft colloid-like behavior. *Macromolecules* 2015, 48, 2305-2312.

3. Glynos, E.; Frieberg, B.; Green, P. F. Wetting of a multiarm star-shaped molecule. *Phys. Rev. Lett.* 2011, 107, 118303.
4. Glynos, E.; Chremos, A.; Frieberg, B.; Sakellariou, G.; Green, P. F. Wetting of macromolecules: From linear chain to soft colloid-like behavior. *Macromolecules* 2014, 47, 1137-1143.

5. Frieberg, B.; Glynos, E.; Sakellariou, G.; Green, P. F. Physical aging of star-shaped macromolecules. *ACS Macro Lett.* 2012, 1, 636-640.

6. Frieberg, B.; Glynos, E.; Green, P. F. Structural relaxations of thin polymer films. *Phys. Rev. Lett.* 2012, 108, 268304.

7. Vlassopoulos, D. Colloidal star polymers: Models for studying dynamically arrested states in soft matter. *J. Polym. Sci. Pol. Phys.* 2004, 42, 2931-2941.

8. Daoud, M.; Cotton, J. P. Star shaped polymers - A model for the conformation and its concentration-dependence. *J. Phys-Paris* 1982, 43, 531-538.

9. Likos, C. N. Effective interactions in soft condensed matter physics. *Phys. Rep.* 2001, 348, 267-439.

10. Chremos, A.; Glynos, E.; Green, P. F. Structure and dynamical intra-molecular heterogeneity of star polymer melts above glass transition temperature. *The Journal of Chemical Physics* 2015, 142, 044901.

11. Likos, C. N.; Lowen, H.; Watzlawek, M.; Abbas, B.; Jucknischke, O.; Allgaier, J.; Richter, D. Star polymers viewed as ultrasoft colloidal particles. *Phys. Rev. Lett.* 1998, 80, 4450-4453.

12. Vlassopoulos, D.; Pakula, T.; Fytas, G.; Roovers, J.; Karatasos, K.; Hadjichristidis, N. Ordering and viscoelastic relaxation in multiarm star polymer melts. *Europhys. Lett.* 1997, 39, 617-622.

13. Pakula, T. Static and dynamic properties of computer simulated melts of multiarm polymer stars. *Comput. Theor. Polym. S.* 1998, 8, 21-30.

14. Pakula, T.; Vlassopoulos, D.; Fytas, G.; Roovers, J. Structure and dynamics of melts of multiarm polymer stars. *Macromolecules* 1998, 31, 8931-8940.

15. Striolo, A.; Prausnitz, J. M. Adsorption of branched homopolymers on a solid surface. *The Journal of Chemical Physics* 2001, 114, 8565-8572.

16. Minnikanti, V. S.; Archer, L. A. Entropic attraction of polymers toward surfaces and its relationship to surface tension. *Macromolecules* 2006, 39, 7718-7728.

17. Qian, Z. Y.; Minnikanti, V. S.; Sauer, B. B.; Dee, G. T.; Archer, L. A. Surface tension of symmetric star polymer melts. *Macromolecules* 2008, 41, 5007-5013.
18. Kosmas, M. K. Ideal polymer-chains of various architectures at a surface. *Macromolecules* 1990, 23, 2061-2065.

19. Bohme, T. R.; de Pablo, J. J. Evidence for size-dependent mechanical properties from simulations of nanoscopic polymeric structures. *The Journal of Chemical Physics* 2002, 116, 9939-9951.

20. Yoshimoto, K.; Jain, T. S.; Nealey, P. F.; de Pablo, J. J. Local dynamic mechanical properties in model free-standing polymer thin films. *The Journal of Chemical Physics* 2005, 122, 144712.

21. Stafford, C. M.; Vogt, B. D.; Harrison, C.; Julthongpiput, D.; Huang, R. Elastic moduli of ultrathin amorphous polymer films. *Macromolecules* 2006, 39, 5095-5099.

22. Torres, J. M.; Stafford, C. M.; Vogt, B. D. Elastic modulus of amorphous polymer thin films: relationship to the glass transition temperature. *ACS Nano* 2009, 3, 2677-2685.

23. Dequidt, A.; Long, D. R.; Sotta, P.; Sanseau, O. Mechanical properties of thin confined polymer films close to the glass transition in the linear regime of deformation: theory and simulations. *Eur. Phys. J. E* 2012, 35, 61.

24. Domke, J.; Radmacher, M. Measuring the elastic properties of thin polymer films with the atomic force microscope. *Langmuir* 1998, 14, 3320-3325.

25. Watcharotone, S.; Wood, C. D.; Friedrich, R.; Chen, X. Q.; Qiao, R.; Putz, K.; Brinson, L. C. Interfacial and substrate effects on local elastic properties of polymers using coupled experiments and modeling of nanoindentation. *Adv. Eng. Mater.* 2011, 13, 400-404.

26. Xu, W.; Chahine, N.; Sulchek, T. Extreme hardening of PDMS thin films due to high compressive strain and confined thickness. *Langmuir* 2011, 27, 8470-8477.

27. Chung, P. C.; Glynos, E.; Green, P. F. The elastic mechanical response of supported thin polymer films. *Langmuir* 2014, 30, 15200-15205.

28. Chung, P. C.; Green, P. F. The elastic mechanical response of nanoscale thin films of miscible polymer/polymer blends. *Macromolecules* 2015, 48, 3991-3996.

29. Silbernagl, D.; Cappella, B. Mechanical properties of thin polymer films on stiff substrates. *Scanning* 2010, 32, 282-293.

30. Hadjichristidis, N.; Iatrou, H.; Pispas, S.; Pitsikalis, M. Anionic polymerization: High vacuum techniques. *J. Polym. Sci. Pol. Chem.* 2000, 38, 3211-3234.
31. Uhrig, D.; Mays, J. W. Experimental techniques in high-vacuum anionic polymerization. *J. Polym. Sci. Pol. Chem.* 2005, 43, 6179-6222.

32. Hutter, J. L.; Bechhoefer, J. Calibration of atomic-force microscope tips. *Rev. Sci Instrum.* 1993, 64, 1868-1873.

33. Butt, H. J.; Cappella, B.; Kappl, M. Force measurements with the atomic force microscope: Technique, interpretation and applications. *Surf. Sci. Rep.* 2005, 59, 1-152.
34. Passeri, D.; Rossi, M.; Tamburri, E.; Terranova, M. L. Mechanical characterization of polymeric thin films by atomic force microscopy based techniques. *Anal. Bioanal. Chem.* 2013, 405, 1463-1478.

35. Johnson, K. L.; Kendall, K.; Roberts, A. D. Surface Energy and Contact of Elastic Solids. *Proc. R. Soc. Lon. Ser-A* 1971, 324, 301-313.

36. Nielsen, L. E. Mechanical properties of polymers; Van Nostrand Reinhold: New York, 1962.

37. Dokukin, M. E.; Sokolov, I. On the measurements of rigidity modulus of soft materials in nanoindentation experiments at small depth. *Macromolecules* 2012, 45, 4277-4288.

38. Alcoutlabi, M.; McKenna, G. B. Effects of confinement on material behaviour at the nanometre size scale. *J. Phys. Condens Mat.* 2005, 17, R461-R524.

39. Forrest, J. A.; Dalnoki-Veress, K. The glass transition in thin polymer films. *Adv. Colloid Inter.* 2001, 94, 167-196.

40. Xia, W.; Keten, S. Interfacial stiffening of polymer thin films under nanoconfinement. *Extreme Mechanics Letters* 2015, http://dx.doi.org/10.1016/j.eml.2015.05.001.

Chapter 5

Conclusions

The work shown in this dissertation was performed to understand and clarify the factors influencing the elastic mechanical response of supported thin polymer films. Various systems including linear-chain polymers, miscible polymer/polymer/blends, and star-shaped polymers supported by silicon oxide (SiO_x) substrates were investigate using an atomic force microscopy based nanoindentation technique. It is shown that difference in the overall mechanical response of different thin polymer films cannot be solely rationalized in terms of the macroscopic elastic modulus and Poisson's ratio of the individual polymers. Moreover, the mechanical response measured with an indentation technique is insensitive to interfacial interactions between a polymer and external interfaces due to the much larger length scale of actual probing depth (on the order of few hundreds of nanometers) compared to that of interfacial interactions (on the order of few nanometers). Experimental results suggest that information regarding the local vibrational force constant (i.e. the local chain stiffness) of individual polymers is required to rationalize the difference in mechanical response of "*amorphous*" polymers. It is also shown that the molecular architecture influences the mechanical response of thin polymer films. This is attributed to the highly ordered structure form by star-shaped

macromolecules with sufficiently high number of arms and low enough molecular weight per arm.

In chapter 2, thin polymer films including polystyrene (PS), poly(methyl methacrylate), polycarbonate (PC), and poly(vinyl chloride) (PVC) supported by SiO_x substrates were investigated. The effective modulus, *E*, of a polymer film supported by a stiff substrate increases with decreasing film thickness, *h*, for *h* less than a threshold thickness h_t. This is due to the indentation-induced stress field extending throughout the entire film and strongly interacting with the underlying stiff substrate; this is the so-called "substrate effect". The extent of substrate effect was comparable and stronger for PS and PMMA films compares to PC films; the moduli of PVC films were independent of *h* for the values of *h* studied. The macroscopic elastic moduli and Poisson's ratios of the polymers do not provide satisfactory rationalization of the different in the degree of substrate effect. Moreover, the overall mechanical response of supported polymer films appears to be insensitive to interfacial interactions at the free surface and polymer/substrate interface. It is suggested that the overall mechanical response of polymers is strongly correlated with the local vibrational force constants of the polymers.

In chapter 3, a miscible blend system composed of PS and tetramethyl bisphenol-A polycarbonate (TMPC) is investigated in order to further understand the elastic mechanical response of polymeric thin films. The influence of effects associated with the different glass transition temperatures, specific volumes, and interfacial compositions of the blends is not significant on the overall mechanical response. Consistent with the findings in chapter 2, difference in elastic mechanical response of blend films was successfully rationalized in terms of the local vibrational force constants of the blend

systems. This work has shown that the overall mechanical response of polymer films could be understood in terms of the local stiffness in case of amorphous polymers. However, the correlation between the macroscopic modulus and local stiffness of the polymers are not well understood and there are still open questions to be answered.

In chapter 4, a series of star-shaped PS (SPS) films of varying number of arms, f, and molecular weight per arm, M_n^{arm}, is investigated. Consistent with previous studies, E increases with decreasing h for all of the SPS films. However, much stronger degree of enhancement of E was observed for 64-arm SPS molecules with sufficiently small M_n^{arm} compared to SPS molecules with lower f and 64-arm stars with larger values of M_n^{arm}. It is suggested that the strong degree of enhancement is associated with the highly order structures of 64-arm SPS molecules with small enough M_n^{arm}.

Appendix A

A.1 Analysis of nanoindentation data with the DMT model

Same set of force-distance curves obtained from polystyrene (PS) and tetramethyl bisphenol-A polycarbonate (TMPC) is also analyzed with the Derjaguin-Muller-Toporov (DMT) model [1], and the data are compared with those analyzed with the Johnson-Kendall-Roberts (JKR) [2] in Figure A.1. Estimated values of K are consistently lower than those estimated using the JKR model. Despite the slight differences in the values of K estimated with the JKR and DMT models, the trends of overall elastic mechanical responses are virtually identical.

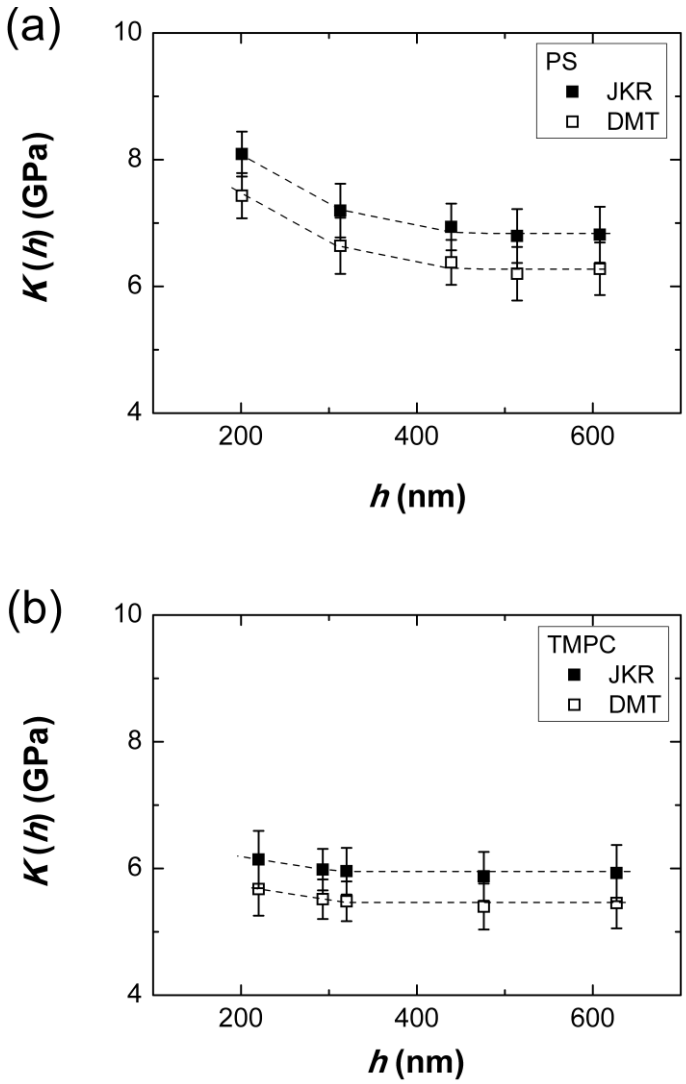

Figure A.1 Effective reduced moduli, $K(h)$, for (a) polystyrene and (b) tetramethyl bisphenol-A polycarbonate (TMPC) estimated by fitting force-distance curves with two different elastic contact models; the JKR (filled squares) and the DMT (open squares). The maximum force, F_{max}, was kept at a constant value of 400 nN for all the measurements. Each data point is an average of 15 nanoindentation measurements, and dashed lines are guides for the eyes.

A.2 References

1. Derjaguin, B. V.; Muller, V. M.; Toporov, Y. P. Effect of contact deformations on adhesion of particles. *J. Colloid Interf. Sci.* 1975, *53*, 314-326.

2. Johnson, K. L.; Kendall, K.; Roberts, A. D. Surface energy and contact of elastic solids. *Proc. R. Soc. Lon. Ser-A* **1971,** *324*, 301-313.

Appendix B

AFM Nanoindentation Experiment

B.1 Nanoindentation Experimental Procedure

1. Place a mica substrate on to the sample holder and purge the sample holder with argon gas in order to minimize the effect of moisture. Set the temperature of the sample holder to 30 ℃; temperature of the sample holder increases to about 28~29 ℃ due to heat from the AFM head.

2. Load an AFM probe on to the AFM probe holder and attach the holder on to the AFM head. After aligning the laser spot, let the deflection and lateral thermally equilibrate. It could take up to few hours.

3. Set the Force Mode to “Closed Loop” in order to maintain constant indentation rate.

3. Calibrate Inverse Optical Lever Sensitivity (InvOLS) of the AFM cantilever on the mica substrate. It is suggested to calibrate the InvOLS with the actual force distance and rate values those will be used for the measurements.

4. After calibration, click Initialize Fit to capture Thermal Data to estimate the spring constant of the AFM cantilever. Wait until 1000 sample count and click stop. The spring constant can be estimated by clicking Fit Thermal Data.

5. Save the calibrated experiment file in case of unexpected malfunctioning. If the AFM computer freezes or in case of black out, one can open the calibrated experiment file to resume experiment. If one moved the laser spot or took off the probe from the holder, the cantilever needs to be re-calibrated.

6. In the commend window, type in "SpotGrid (X,X)"; X can be any positive number. For example, if you set the scan size 9 μm x 9 μm and X as 10, a 10 by 10 grid will be created with each point 1 μm apart from next or prior points. One can move from a point to next using Go There function. Simply changing X and Y offset on the Main tab would not move the position of the tip.

7. Once experiments are done, export raw deflection vs. Z displacement data as text files for analysis.

B.2 Estimating effective modulus from force-distance curves

The effective modulus can be estimated from force-distance (FD) curves with an appropriate contact mechanics models introduced in section 1.2.2. In this work, a customized Matlab code was used to import the raw deflection vs. Z displacement data and converted to force vs. distance using equation 1.1 and 1.2. Both the effective modulus and indentation depth was estimated using the least-squares method. Typically, modulus values from 10 to 15 FD curves were averaged for each sample.